



This is the accepted manuscript made available via CHORUS. The article has been published as:

Onset of collectivity for argon isotopes close to $m_{\text{N}}/m_{\text{O}} \geq m_{\text{N}}/m_{\text{N}} > 32$

B. D. Linh et al.

Phys. Rev. C **109**, 034312 — Published 19 March 2024

DOI: [10.1103/PhysRevC.109.034312](https://doi.org/10.1103/PhysRevC.109.034312)

Onset of collectivity for Argon isotopes close to $N = 32$

B.D. Linh,^{1,2} A. Corsi,³ A. Gillibert,³ A. Obertelli,^{3,4,5} P. Doornenbal,⁴ C. Barbieri,^{6,7} T. Duguet,^{3,8}
M. Gómez-Ramos,⁹ J.D. Holt,^{10,11} B.S. Hu,¹⁰ T. Miyagi,^{5,12,13} A.M. Moro,^{9,14} P. Navrátil,¹⁰ K. Ogata,^{15,16} S.
Péru,^{17,18} N.T.T. Phuc,^{19,20} N. Shimizu,^{21,22} V. Somà,³ Y. Utsuno,^{22,23} N. L. Achouri,²⁴ H. Baba,⁴ F. Browne,⁴
D. Calvet,³ F. Château,³ S. Chen,^{4,25,26} N. Chiga,⁴ M. L. Cortés,⁴ A. Delbart,³ J.-M. Gheller,³ A. Giganon,³
C. Hilaire,³ T. Isobe,⁴ T. Kobayashi,²⁷ Y. Kubota,^{4,22} V. Lapoux,³ H. N. Liu,^{3,5,28} T. Motobayashi,⁴
I. Murray,^{4,29} H. Otsu,⁴ V. Panin,⁴ N. Paul,^{3,30} W. Rodriguez,^{4,31,32} H. Sakurai,^{4,33} M. Sasano,⁴
D. Steppenbeck,⁴ L. Stuhl,^{22,34,35} Y. L. Sun,^{3,5} Y. Togano,³⁶ T. Uesaka,⁴ K. Wimmer,^{4,33} K. Yoneda,⁴
O. Aktas,²⁸ T. Aumann,^{5,37} L.X. Chung,² F. Flavigny,^{24,29} S. Franchoo,²⁹ I. Gašparić,^{4,5,38} R.B. Gerst,³⁹
J. Gibelin,²⁴ K.I. Hahn,^{40,35} N.T. Khai,¹ D. Kim,^{40,4,35} T. Koiwai,³³ Y. Kondo,⁴¹ P. Koseoglou,^{5,37,42} J. Lee,²⁵
C. Lehr,⁵ T. Lokotko,²⁵ M. MacCormick,²⁹ K. Moschner,³⁹ T. Nakamura,⁴¹ S.Y. Park,^{40,35} D. Rossi,⁵
E. Sahin,⁴³ D. Sohler,³⁴ P.-A. Söderström,^{5,44} S. Takeuchi,⁴¹ H. Törnqvist,^{5,37} V. Vaquero,⁴⁵ V. Wagner,⁵
S.T. Wang,⁴⁶ V. Werner,^{5,42} X. Xu,²⁵ Y. Yamada,⁴¹ D. Yan,⁴⁶ Z. Yang,⁴ M. Yasuda,⁴¹ and L. Zanetti⁵

¹ Vietnam Agency for Radiation and Nuclear Safety, 113 Tran Duy Hung, Cau Giay, Hanoi 100000, Vietnam

² Institute for Nuclear Science & Technology, VINATOM, 179 Hoang Quoc Viet, Cau Giay, Hanoi, Vietnam

³ Université Paris-Saclay, IRFU, CEA, F-91191 Gif-sur-Yvette, France

⁴ RIKEN Nishina Center, 2-1 Hirosawa, Wako, Saitama 351-0198, Japan

⁵ Institut für Kernphysik, Technische Universität Darmstadt, 64289 Darmstadt, Germany

⁶ Dipartimento di Fisica "Aldo Pontremoli", Università degli Studi di Milano, Via Celoria 16, I-20133 Milano, Italy

⁷ INFN, Sezione di Milano, Via Celoria 16, I-20133 Milano, Italy

⁸ KU Leuven, Instituut voor Kern- en Stralingsfysica, B-3001 Leuven, Belgium

⁹ Departamento de Física Atomica Molecular y Nuclear, Facultad de Física, Universidad de Sevilla, Apartado 1065, E-41080 Sevilla, Spain

¹⁰ TRIUMF, 4004 Wesbrook Mall, Vancouver, British Columbia V6T 2A3, Canada

¹¹ Department of Physics, McGill University, 3600 Rue University, Montréal, QC H3A 2T8, Canada

¹² ExtreMe Matter Institute EMMI, GSI Helmholtzzentrum für Schwerionenforschung GmbH, 64291 Darmstadt, Germany

¹³ Max-Planck-Institut für Kernphysik, Saupfercheckweg 1, 69117 Heidelberg, Germany

¹⁴ Instituto Interuniversitario Carlos I de Física Teórica y Computacional (iC1), Apdo. 1065, E-41080 Sevilla, Spain

¹⁵ Department of Physics, Kyushu University, Fukuoka 819-0395, Japan

¹⁶ Research Center for Nuclear Physics (RCNP), Osaka University, Ibaraki 567-0047, Japan

¹⁷ CEA, DAM, DIF, F-91297 Arpajon, France

¹⁸ Université Paris-Saclay, CEA, LMCE, 91680 Bruyères-le-Châtel, France

¹⁹ Department of Nuclear Physics, Faculty of Physics and Engineering

Physics, University of Science, Ho Chi Minh City 700000, Vietnam

²⁰ Vietnam National University, Ho Chi Minh City 700000, Vietnam

²¹ Center for Computational Sciences, University of Tsukuba, 1-1-1 Tenno-dai, Tsukuba, 305-8577 Japan

²² Center for Nuclear Study, University of Tokyo, RIKEN campus, Wako, Saitama 351-0198, Japan

²³ Japan Atomic Energy Agency, Tokai, Ibaraki 319-1195, Japan

²⁴ LPC Caen, Normandie Univ, ENSICAEN, UNICAEN, CNRS/IN2P3, F-14000 Caen, France

²⁵ Department of Physics, The University of Hong Kong, Pokfulam 999077, Hong Kong

²⁶ State Key Laboratory of Nuclear Physics and Technology, Peking University, Beijing 100871, China

²⁷ Department of Physics, Tohoku University, Sendai 980-8578, Japan

²⁸ Department of Physics, Royal Institute of Technology, SE-10691 Stockholm, Sweden

²⁹ Université Paris-Saclay, CNRS/IN2P3, IJCLab, Orsay, France

³⁰ Laboratoire Kastler Brossel, Sorbonne Université, CNRS, ENS, PSL Research

University, Collège de France, Case 74, 4 Place Jussieu, F-75005 Paris, France

³¹ Departamento de Física, Pontificia Universidad Javeriana, Bogotá, Colombia

³² Departamento de Física, Facultad de Ciencias, Universidad Nacional de Colombia, Sede Bogotá, Bogotá 111321, Colombia

³³ Department of Physics, University of Tokyo, 7-3-1 Hongo, Bunkyo, Tokyo 113-0033, Japan

³⁴ Institute for Nuclear Research, Atomki, P.O. Box 51, Debrecen H-4001, Hungary

³⁵ Institute for Basic Science, Daejeon 34126, Korea

³⁶ Department of Physics, Rikkyo University, 3-34-1 Nishi-Ikebukuro, Toshima, Tokyo 172-8501, Japan

³⁷ GSI Helmholtzzentrum für Schwerionenforschung GmbH, Planckstr. 1, 64291 Darmstadt, Germany

³⁸ Ruder Bošković Institute, Bijenička cesta 54, 10000 Zagreb, Croatia

³⁹ Institut für Kernphysik, Universität zu Köln, D-50937 Köln, Germany

⁴⁰ Ewha Womans University, Seoul 03760, Korea

⁴¹ Department of Physics, Tokyo Institute of Technology, 2-12-1 O-okayama, Meguro, Tokyo 152-8551, Japan

⁴² Helmholtz Forschungsakademie Hessen für FAIR (HFHF), GSI Helmholtzzentrum

für Schwerionenforschung, Campus Darmstadt, 64289 Darmstadt, Germany

⁴³ Department of Physics, University of Oslo, N-0316 Oslo, Norway

⁶¹ ⁴⁴*Extreme Light Infrastructure-Nuclear Physics (ELI-NP)/Horia Hulubei National Institute for Physics*
⁶² *and Nuclear Engineering (IFIN-HH), Str. Reactorului 30, Bucharest-Măgurele 077125, Romania*

⁶³ ⁴⁵*Instituto de Estructura de la Materia, CSIC, E-28006 Madrid, Spain*

⁶⁴ ⁴⁶*Institute of Modern Physics, Chinese Academy of Sciences, Lanzhou 730000, China*

The shell closure at $N = 32$ has been investigated by a first spectroscopy of the $N = 31$ nucleus ⁴⁹Ar at the Radioactive Isotope Beam Factory. Using the ⁵⁰Ar(p,pn) reaction channel in inverse kinematics, ⁵⁰Ar projectiles at 217 MeV/nucleon impinged on a 150 mm long liquid hydrogen target, part of the MINOS device. Prompt de-excitation γ rays were measured with the NaI(Tl) array DALI2⁺. Reaction products were analyzed with the SAMURAI spectrometer, which allowed the measurement of the momentum distributions and angular momentum transfer. Data are compared to state-of-the-art theoretical predictions, including shell model, energy-density functional, and *ab initio* calculations. An onset of collectivity is suggested besides the spherical configuration typical of a closed shell nucleus, such as for ⁵²Ca.

⁶⁵ I. INTRODUCTION

⁶⁶ The neutron number $N = 28$ is considered a magic
⁶⁷ number corresponding, in the standard shell-model pic-
⁶⁸ ture, to a filled neutron $\nu 0f_{7/2}$ orbital and a well-defined
⁶⁹ energy gap. For stable nuclei, the main evidence of this
⁷⁰ shell closure is given by ⁴⁸Ca combining observations
⁷¹ from mass measurements, γ -ray spectroscopy, or transfer
⁷² measurements [1]. However, shell closures evolve across
⁷³ the nuclear chart as a result of the delicate balance be-
⁷⁴ tween the different correlations at play among the nucle-
⁷⁵ ons. For instance, when more proton-deficient $N = 28$
⁷⁶ isotones are considered, an onset of quadrupole deforma-
⁷⁷ tion is observed for nuclei such as ⁴²Si [2–4] or ⁴⁰Mg [5].
⁷⁸ In contrast, $N = 32$ and 34 have been proposed to be
⁷⁹ new magic numbers [6], not observed for stable nuclei,
⁸⁰ corresponding to filled $\nu 1p_{3/2}$ and $\nu 1p_{1/2}$ orbitals, re-
⁸¹ spectively.

⁸² Mass excesses for neutron-rich nuclei have been de-
⁸³ termined for Ca isotopes [7–9] up to ⁵⁷Ca. The char-
⁸⁴ acteristic behavior of the two-neutron separation energy
⁸⁵ S_{2n} at a major shell closure - relatively flat below and
⁸⁶ with a sharp decrease over two neutron units beyond - is
⁸⁷ clearly observed, not only at $N = 28$ but also at $N = 32$
⁸⁸ for ⁵²Ca. This closure effect, shown by the global ob-
⁸⁹ servable S_{2n} , has been confirmed by the measurements
⁹⁰ of the energy $E(2_1^+)$ of the first 2_1^+ state and the re-
⁹¹ duced transition probabilities $B(E2; 0_1^+ \rightarrow 2_1^+)$. A high
⁹² value of $E(2_1^+)$, compared to the neighboring isotopes,
⁹³ was found for ⁴⁸Ca and ⁵²Ca [10, 11]. This was further
⁹⁴ confirmed by the low values of $E(2_1^+)$ recently measured
⁹⁵ in ^{56,58}Ca [12]. A small $B(E2; 0_1^+ \rightarrow 2_1^+)$ value was found
⁹⁶ for ⁴⁸Ca [13, 14], but is still missing for ⁵²Ca. Unex-
⁹⁷ pected for a closed-shell nucleus, the large increase of
⁹⁸ the ⁵²Ca charge radius [15], compared to ⁴⁸Ca, is now
⁹⁹ rather assigned to a larger radius of the $\nu 1p_{3/2}$ orbital
¹⁰⁰ and isovector polarizability [16, 17]. Additional converg-
¹⁰¹ ing information is provided by the analyses of neutron
¹⁰² transfer reactions [18, 19]. For ⁴⁷Ca, the $7/2_1^-$ ground
¹⁰³ state has a large spectroscopic factor C^2S , close to the
¹⁰⁴ $2j + 1$ limit compatible with a neutron hole state in the
¹⁰⁵ $\nu 0f_{7/2}$ orbital in ⁴⁸Ca. At the same time, small C^2S
¹⁰⁶ values were found for the $3/2^-$ states, consistent with
¹⁰⁷ little occupancy of the $\nu 1p_{3/2}$ orbital. Such information

¹⁰⁸ was still missing for ⁵²Ca until a recent analysis of the
¹⁰⁹ ⁵²Ca(p,pn) knockout [16].

¹¹⁰ These experimental results are strong enough to estab-
¹¹¹ lish the concept of a shell closure for ⁴⁸Ca at $N = 28$,
¹¹² and arguably for ⁵²Ca at $N = 32$. However, such proper-
¹¹³ ties may not be as robust for light nuclei as they are for
¹¹⁴ heavier nuclei where, for instance, $N = 82$ or 126 magic
¹¹⁵ gaps are well established over a large range of atomic
¹¹⁶ number Z . For isotopic series with $Z > 20$, a similar
¹¹⁷ - although weakening with increasing Z - behavior has
¹¹⁸ been observed for both $N = 28$ and $N = 32$ in tita-
¹¹⁹ nium and chromium nuclei [20–22], with higher $E(2_1^+)$
¹²⁰ and smaller $B(E2; 0_1^+ \rightarrow 2_1^+)$ values.

¹²¹ The isotopic distributions with $Z < 20$, such as the
¹²² argon distribution, are less documented since they corre-
¹²³ spond to more neutron-rich nuclei. Mass measurements
¹²⁴ have extended the S_{2n} evolution to neutron-rich argon
¹²⁵ isotopes and are consistent with a shell closure at $N =$
¹²⁶ 28 [23, 24]. A low $B(E2; 0_1^+ \rightarrow 2_1^+)$ value was also found
¹²⁷ for ⁴⁶Ar [13, 25]. This value increases for ⁴⁸Ar [26] but is
¹²⁸ missing for more neutron-rich isotopes. High $E(2_1^+)$ val-
¹²⁹ ues have been determined by in-beam γ -ray spectroscopy
¹³⁰ for ⁴⁶Ar [13] and ⁵²Ar [27], while $E(2_1^+)$ for ⁵⁰Ar [28, 29]
¹³¹ is comparatively reduced. However, the link between
¹³² $E(2_1^+)$ and a shell closure effect may be discussed. In
¹³³ shell model calculations performed with the SDPF-MU
¹³⁴ interaction [28], the 2_1^+ state for ⁵²Ca is understood as a
¹³⁵ neutron excitation $\nu 1p_{3/2} \rightarrow \nu 1p_{1/2}$ from a ground state
¹³⁶ dominated by a $(\nu 1p_{3/2})^4$ configuration (about 90%).
¹³⁷ Therefore, in this case, the large value of $E(2_1^+)$ is rep-
¹³⁸ resentative of the $N = 32$ energy gap. When removing
¹³⁹ two protons, the same calculation predicts for ⁵⁰Ar mixed
¹⁴⁰ configurations for the 0_1^+ , 2_1^+ , and 4_1^+ states, such that
¹⁴¹ $E(2_1^+)$ is not so cleanly connected to the monopole en-
¹⁴² ergy gap. Furthermore, the analysis of the neutron pick-
¹⁴³ up at $N = 28$ ⁴⁶Ar(d,p)⁴⁷Ar reaction suggests a partial
¹⁴⁴ occupation of the $\nu 0f_{7/2}$ orbital, while the spectroscopic
¹⁴⁵ factors of the $3/2^-$ states are consistent with a substan-
¹⁴⁶ tial occupancy of the $\nu 1p_{3/2}$ orbital [30]. Going further
¹⁴⁷ with the quadrupolar degree of freedom, theoretical cal-
¹⁴⁸ culations such as energy-density functional calculations
¹⁴⁹ feature shapes away from spherical [31, 32] with compe-
¹⁵⁰ tition between oblate and prolate minima, when protons
¹⁵¹ are removed from Ca isotopes. This results, for example,

152 in a weak oblate minimum predicted for the ground state
 153 of ^{46}Ar , but a dominant one for ^{42}Si , with a low $E(2_1^+)$
 154 value measured for the latter [2–4]. The potential energy
 155 surfaces obtained for the $N = 32$ isotones ^{50}Ar , ^{48}S , and
 156 ^{46}Si in mean-field calculations with the Gogny effective
 157 interaction [33–35] are consistent with rather soft nuclei
 158 against quadrupole deformation.

159 To get a better insight into the robustness of the sub-
 160 shell closure at $N = 32$, the one-neutron knockout re-
 161 action $^{50}\text{Ar}(p,pn)^{49}\text{Ar}$ has been used to provide infor-
 162 mation on hole states from the ^{50}Ar core. The aim is
 163 to determine the excitation energy and cross sections of
 164 the low-lying states in ^{49}Ar . Experimental data are com-
 165 pared to state-of-the-art theoretical predictions, includ-
 166 ing shell model, energy-density functional, and *ab initio*
 167 calculations. In particular, the shell model calculations
 168 also serve as a guideline for the experimental analysis.

169 This article is structured as follows. The experimen-
 170 tal setup is described in Section II. The methods used
 171 for data analysis are developed in Section III, including
 172 the determination of momentum distributions and cross
 173 sections. In the same experiment, a similar analysis has
 174 been performed on the isotopes $^{47,49}\text{Cl}$, which was ex-
 175 tensively described in Ref. [36]. Therefore, here only the
 176 main features are recalled. A presentation of the experi-
 177 mental results for ^{49}Ar concludes Section III. Finally, an
 178 extensive discussion of the experimental findings and the
 179 theoretical calculations is the object of Section IV.

180 II. EXPERIMENTAL SETUP

181 The experiment was performed at the Radioactive
 182 Isotope Beam Factory (RIBF), operated jointly by the
 183 RIKEN Nishina Center and the Center for Nuclear Study
 184 of the University of Tokyo. A ^{70}Zn beam was accelerated
 185 up to 345 MeV/nucleon for the production of a mixed sec-
 186 ondary beam, including the ^{50}Ar beam, selected with the
 187 help of the BigRIPS separator [37] and identified with the
 188 magnetic rigidity $B\rho$, energy loss ΔE , and time of flight
 189 TOF measurements [38]. Within the MINOS setup [39],
 190 a 151(1) mm thick liquid hydrogen target was used to
 191 compensate for the low-intensity beams.

192 The incident energy at the entrance (exit) of the sec-
 193 ondary target was ~ 247 (~ 184) MeV/nucleon, with an
 194 intensity of 2.9 particles/s for ^{50}Ar . The scattered ions
 195 were analyzed with the SAMURAI large acceptance spec-
 196 trometer [40] behind the secondary target and identified
 197 by the mass-over-charge ratio A/Q and the atomic num-
 198 ber Z . The unambiguous separation of the different pro-
 199 jectiles and residues is shown in Fig. 1. Prompt gamma-
 200 rays emitted at the MINOS target were detected with
 201 the DALI2⁺ array [41], composed of 226 NaI(Tl) detec-
 202 tors in a compact geometry. The target was surrounded
 203 by the cylindrical time-projection chamber of the MINOS
 204 setup [39], which was used for the determination of the
 205 reaction vertex and the Doppler-shift correction. The en-
 206 ergy calibration of the DALI2⁺ array and the procedure

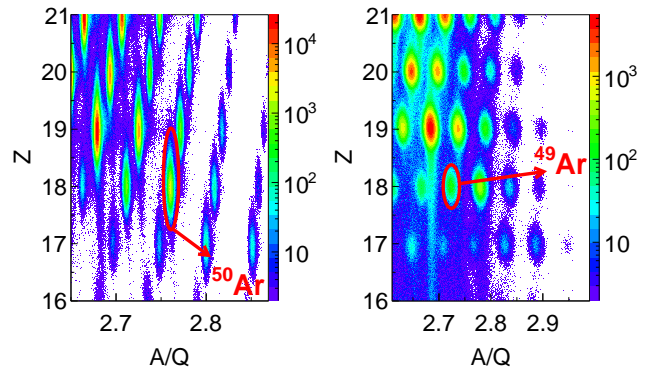


FIG. 1. Particle identification with the mass over charge ra-
 tio number A/Q and atomic number Z : (left) beam particle
 identification at BigRIPS before the target; (right) residue
 particle identification downstream of the secondary target
 from the large acceptance SAMURAI spectrometer. ^{50}Ar and ^{49}Ar
 in front and behind the MINOS secondary target are shown
 by the red ellipses.

207 for Doppler-shift correction due to in-flight emission are
 208 given in Ref. [36].

209 III. SPECTROSCOPY OF ^{49}Ar

210 Different reaction channels have been used to study
 211 the bound states in ^{49}Ar below the one-neutron sepa-
 212 ration energy $S_n = 2780$ (400) keV [42]: *i*) $^{50}\text{Ar}(p,pn)$
 213 which is expected to populate single particle states by
 214 one-neutron knockout from the ^{50}Ar core; *ii*) $^{51}\text{K}(p,2pn)$
 215 with a more complex reaction mechanism possibly popu-
 216 lating states at higher spin and higher excitation energy;
 217 *iii*) inelastic scattering $^{49}\text{Ar}(p,p')$ which favors the exci-
 218 tation of collective states from the ground state. The cor-
 219 responding Doppler-corrected energy spectra are shown
 220 in Fig. 2(a) and (b) after subtraction of a low-energy
 221 background component. This subtraction explained in
 222 Ref. [36], was also applied here since a low-energy tran-
 223 sition was observed in ^{49}Ar at 198 keV: The low-energy
 224 bremsstrahlung component from the $^{49}\text{Ar}(p,p)$ scattering
 225 is normalized and subtracted in the spectra, except for
 226 the same channel in Fig. 2(c). Then, the single spectra
 227 were reproduced by a combination of response functions
 228 for transitions and a two-component exponential back-
 229 ground with fitted amplitudes.

230 A. $^{50}\text{Ar}(p,pn)^{49}\text{Ar}$

231 In a shell-model picture, the one-neutron knockout re-
 232 action is expected to populate states in ^{49}Ar , which have
 233 a sizable overlap with the neutron-hole configurations
 234 $(\nu 1p_{3/2})^{-1}$ and $(\nu 0f_{7/2})^{-1}$, assuming these orbitals to

235 be filled in the $N = 32$ isotope ^{50}Ar . For a closed-shell
 236 nucleus, the $\nu 1p_{1/2}$ orbital should be nearly empty, re-
 237 sulting in a weak population of $1/2^-$ states in this direct
 238 reaction.

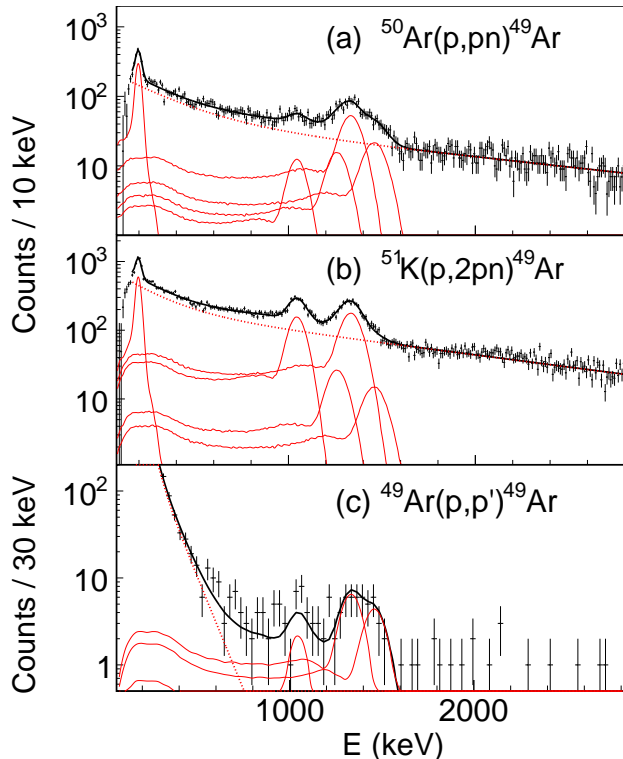


FIG. 2. Doppler-corrected γ -ray spectra of ^{49}Ar obtained from a) one-neutron knockout $^{50}\text{Ar}(p,pn)$, b) the more complex $^{51}\text{K}(p,2pn)$ reaction and c) inelastic scattering $^{49}\text{Ar}(p,p')$. Spectra in a) and b) are obtained after subtraction of a low-energy bremsstrahlung component (see text). Experimental data (points) are fitted by a combination (black line) of five simulated DALI2⁺ response functions (red continuous lines) and a two-component exponential background (red dashed line).

239 The one-neutron knockout spectrum in Fig. 2a) dis-
 240 plays an intense peak at 198 keV and a broad structure
 241 between 900 and 1600 keV on top of the background.
 242 There is no strong evidence for another transition at
 243 higher energy. The broad structure is reproduced mainly
 244 by three response functions corresponding to transitions
 245 at 1050, 1340, and 1466 keV.

246 $\gamma - \gamma$ correlations have also been examined with gates
 247 corresponding to the main transitions observed in the
 248 singles spectrum. No clear coincidence was observed in
 249 this first step. Then, a different procedure was used
 250 to determine a possible coincidence with the 198 keV
 251 transition due to the complex underlying Compton back-
 252 ground. A moving gate was applied over the whole en-
 253 ergy spectrum while searching for the 198 keV transition
 254 and a significant coincidence with a confidence level of
 255 5.5σ was found for the energy gate [1180,1320] keV as

256 shown in Fig. 3(a). Due to fluctuations, no other transi-
 257 tion could be significantly identified. No coincidence was
 258 found for gates at higher energies, dominated by the 1340
 259 and 1466 keV transitions. An other spectrum is shown
 260 in Fig. 3(b) corresponding to the gates just below and
 261 above the [1180,1320] gate.

262 This is an indication of a possible coincidence between
 263 the transitions at 188 and 1266 keV, the latter being not
 264 clearly visible in the singles spectrum due to the over-
 265 whelming 1340 keV transition nearby. The summed en-
 266 ergy of the coincidence is 1464 keV, consistent with the
 267 observed transition at 1466(21) keV. So it was included
 268 for the fits of the singles spectra of Fig. 2, even if its
 269 weight was dominated by the 1340 keV transition. Ad-
 270 ditionally, this 1266 keV transition was useful for repro-
 271 ducing the left side of the wide bump around 1300 keV.

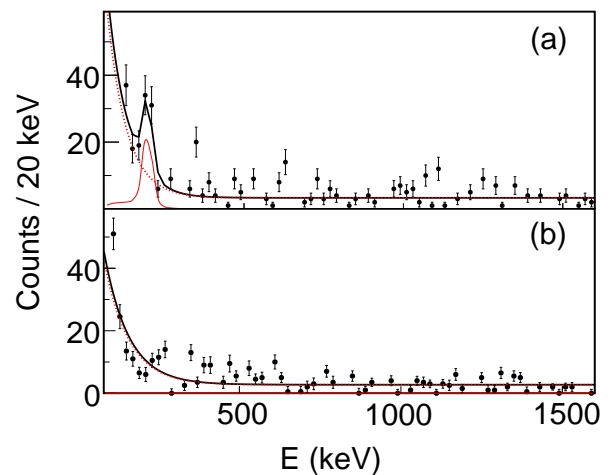


FIG. 3. Doppler-corrected γ -ray spectra of ^{49}Ar obtained from the one-neutron knockout $^{50}\text{Ar}(p,pn)$ a) gated by the [1180,1320] range in Fig. 2 a) which maximizes the ratio of the response function corresponding to the 1266 keV transition over other transitions; b) gated by the energy ranges just below and above which maximizes the background due to other transitions.

272 The overlap of the Compton spectra included in the
 273 different response functions was sufficient to reproduce
 274 correctly the energy range between 200 and 900 keV with-
 275 out evidence for another strong transition.

276 Finally, the simplest reproduction of the histogram
 277 shown in Fig. 2 (a) was obtained by a combination of re-
 278 sponse functions at 198(3), 1050(29), 1266(41), 1340(14),
 279 and 1466(21) keV, on top of a two-component exponen-
 280 tial background.

281 The inelastic scattering $^{50}\text{Ar}(p,p')$ can populate col-
 282 lective states in ^{50}Ar above the one-neutron separation
 283 energy $S_n = 4210$ keV, which will decay and popu-
 284 late low lying states in ^{49}Ar . In the previous analysis,
 285 this contribution cannot be distinguished from the di-
 286 rect one-neutron removal reaction channel, except for the

neutron emitted at a very forward angle and detected with the NEULAND demonstrator [43] and the NEBULA array [44]. Similar analyses were already performed in [16, 45] and the contribution was subtracted from the cross sections below.

B. Other reaction channels

TABLE I. Transitions observed in Fig. 2 for the two different reaction channels $^{50}\text{Ar}(p,pn)^{49}\text{Ar}$ and $^{51}\text{K}(p,2pn)^{49}\text{Ar}$: Excitation energy E^* , detection-efficiency corrected intensity I_i and intensity ratios normalized to the 1050 and 1340 keV transitions.

E^* (keV)	$^{50}\text{Ar}(p,pn)^{49}\text{Ar}$			$^{51}\text{K}(p,2pn)^{49}\text{Ar}$		
	$I_i/10^3$	$\frac{I_i}{I_{1340}}$	$\frac{I_i}{I_{1050}}$	$I_i/10^3$	$\frac{I_i}{I_{1340}}$	$\frac{I_i}{I_{1050}}$
198(3)	1.68(9)	0.65(6)	3.55	3.51(15)	0.40(2)	0.60
1050(29)	0.47(11)	0.18(4)	1.	5.84(24)	0.67(4)	1.
1266(41)	0.75(17)	0.29(7)	1.59	1.42(29)	0.16(3)	0.24
1340(14)	2.58(19)	1.	5.45	8.73(33)	1.	1.50
1466(21)	1.22(14)	0.47(7)	2.58	1.02(22)	0.12(3)	0.17

293

A similar analysis has been performed for the $^{51}\text{K}(p,2pn)^{49}\text{Ar}$ channel in Fig. 2(b), using the response functions with the same centroid energies obtained for the $^{50}\text{Ar}(p,pn)^{49}\text{Ar}$ reaction. They were sufficient to reproduce the experimental spectrum, with no evidence of another strong transition.

Compared to the intensity of the 1340 keV transition, one observes an intensity reduction of the 1466 keV transition and a strong intensity enhancement of the 1050 keV transition. This enhancement is consistent with the decay of a state which would be less populated in the direct neutron knockout, due to a small overlap with a neutron-hole configuration, than in a more complex reaction channel favoring a population of higher spin or higher-lying states. The intensity ratios I_i/I_{1050} are shown in Tab. I. The four other transitions are clearly enhanced in the one-neutron knockout. There was no evidence of a transition in coincidence with the 1050 keV transition.

The inelastic scattering channel $^{49}\text{Ar}(p,p')$ is shown in Fig. 2 (c). In order to display all the statistics for high-energy photons, the vertex reconstruction was not used here. The low-energy background subtraction procedure with the unreacted beam, used for all the other channels, could not be applied in this case. In spite of the dominance of the low energy component below 500 keV and low statistics above, there is evidence for γ rays with energies larger than 800 keV. We see that two response functions corresponding to the transitions at 1340 and 1466 keV observed previously may explain the high energy part around 1400 keV. The region between 700 and

1200 keV is more uncertain due to either (i) a possible tail of the low-energy background not fully reproduced, (ii) the contribution of the transition at 1050 keV, or (iii) decays of unresolved collective states populated in the scattering. At this step, we can only say that these transitions originate from the decay of states populated by collective nuclear excitations from the ground state. An example is proposed in the shell model calculation using the SDPF-MUs interaction [46] with the $3/2_1^- \rightarrow 7/2_1^-$ excitation and the largest value $B(E2) \uparrow = 103 e^2 fm^4$ obtained for $E2$ excitation from the $3/2_1^-$ ground state. Finally, with limited statistics, the minimal assumption of three response functions at 1050, 1340, and 1466 keV over the low-energy background is enough to reproduce data in Fig. 2(c).

339

C. Momentum distributions

Due to the large acceptance of the magnetic spectrometer SAMURAI, most of the charged reaction products and unreacted beams were measured in the detectors used for the reconstruction of momentum distributions, as explained in Ref. [36]. The exclusive parallel (PMD) and transverse p_x (TMD) momentum distributions are seen in Fig. 4 with a 40 MeV/c binning corresponding to the experimental resolution. For each bin, the amplitudes of the response functions from Fig. 2 (a) were determined. Then, the distributions were normalized through the experimental cross sections associated with these transitions. For each transition, there is an underlying Compton background in the spectrum from higher-lying response functions and from other unresolved transitions. It may introduce some uncertainty on the intensity of the momentum bin due to possible contributions from other ℓ -values, especially for the lowest-energy transitions, such as the 198 keV transition. Due to the limited statistics, momentum distributions could only be determined for the most intense transitions at 198 and 1340 keV.

For the one neutron knockout channel, these distributions are sensitive to the orbital angular momentum ℓ of the knocked-out nucleon and can be compared to distributions obtained from various reaction models. Besides the popular choice of distorted-wave-impulse-approximation (DWIA) [48, 49], we also used the transfer to continuum method (TC) [47], as shown in Fig. 4 for p and f waves, with very similar results. The slight asymmetry observed in parallel momentum distributions is a phase space effect due to energy and momentum conservation [50].

371

The distributions (a) and (c) obtained for the 198 keV transition are consistent with an $\ell = 1$ knocked-out neutron, narrower than the $\ell = 3$ distribution, in spite of weak possible ℓ -background. With only the ℓ value, it was not possible to determine the spin-parity of a 198

372

373

374

375

376

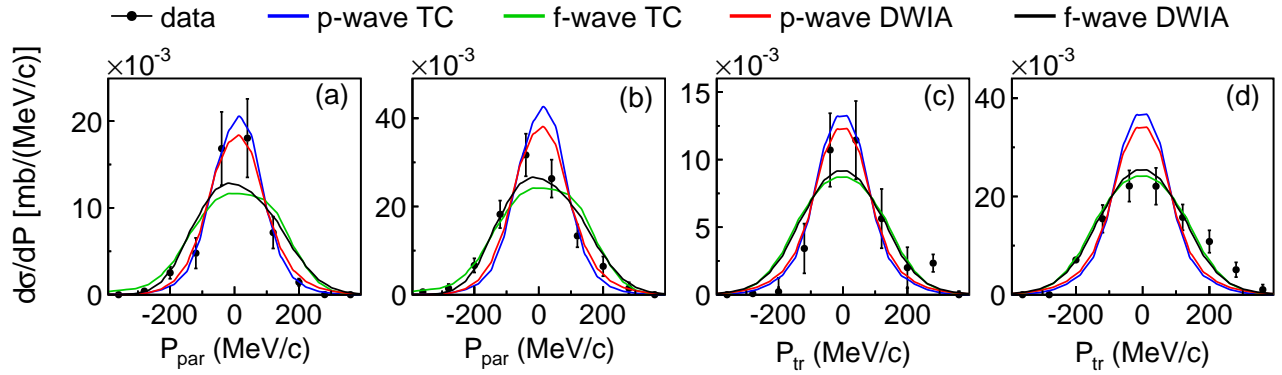


FIG. 4. Momentum distributions of ^{49}Ar ejectiles following the one-neutron knockout reaction: a) and b) PMD in coincidence with the 198 and 1340 keV transitions measured in DALI2⁺; c) and d) TMD in coincidence with the 198 and 1340 keV transitions. Data are compared to calculations with the TC [47] and DWIA [48] methods for $\ell = 1$ and $\ell = 3$ waves after convolution with the experimental resolution.

TABLE II. Comparison between experimental results and theoretical predictions derived from shell-model calculations with the SDPF-MU_s interaction [46] for the one-neutron knockout reaction $^{50}\text{Ar}(p,pn)$. The excitation energies E_{exp} , cross sections σ_{exp} , and angular momentum transfer $\Delta\ell$ for the listed states in ^{49}Ar are deduced from the experiment. Theoretical cross sections $\sigma_{th,i}$ are obtained from Eq. (1), using the calculated C^2S spectroscopic factors and single-particle cross sections $\sigma_{sp}^{lj}(E^*, E_{inc})$ from the TC [47] and DWIA [48] methods. The states are listed up to the estimated one-neutron separation energy 2780(400) keV [42]. The last three rows compare the total inclusive cross section σ_{inc} to the sum of exclusive experimental cross sections $\sum \sigma_i^{ex}$ and the sum of theoretical cross sections $\sum \sigma_{th,i}$.

Experiment			$\sigma_{sp}^{lj}(E^*, E_{inc})$			SDPF-MUs				
E_{exp} (keV)	σ_{exp} (mb)	$\Delta\ell$	nlj	σ_{TC} (mb)	σ_{DW} (mb)	State	Energy (keV)	C^2S	$\sigma_{th,TC}$ (mb)	$\sigma_{th,DWIA}$ (mb)
gs	<17(3)		$1p_{3/2}$	7.4	7.94	$3/2_1^-$	gs	1.844	13.64	14.64
198(3)	3.0(9)	1	$1p_{1/2}$	7.2	7.53	$1/2_1^-$	94	0.616	4.43	4.64
1050(29)	1.5(3)			5.8	4.69	$5/2_1^-$	923	0.006	0.03	0.03
1340(14)	8.3(7)	3	$0f_{7/2}$	6.1	5.52	$7/2_1^-$	983	2.564	15.64	14.15
1466(21)	6.3(10)		$1p_{3/2}$	6.4	7.15	$3/2_2^-$	1197	0.678	4.34	4.85
			$0f_{5/2}$	5.9	4.59	$5/2_2^-$	1460	0.233	1.37	1.07
			$0f_{5/2}$	5.7	4.49	$5/2_3^-$	2096	0.019	0.11	0.08
			$1p_{3/2}$	5.7	4.47	$3/2_3^-$	2184	0.029	0.16	0.13
						$9/2_1^-$	2267	0.		
			$0f_{7/2}$	5.9	5.21	$7/2_2^-$	2317	0.050	0.29	0.26
			$1p_{1/2}$	5.8	6.22	$1/2_2^-$	2529	0.017	0.10	0.11
			$0f_{7/2}$	5.8	5.14	$7/2_3^-$	2702	0.262	1.52	1.35
			$1p_{3/2}$	5.85	6.37	$3/2_4^-$	2870	0.191	1.12	1.22
						$9/2_2^-$	3044	0.		
			$1p_{1/2}$			$1/2_3^-$	3094	0.000		
σ_{inc}	36.3 (9)							$\sum \sigma_{th,i}$	42.75	42.53
$\sum \sigma_{exp,i}^{ex}$	19.1(18)									

377 keV state, either $3/2^-$ or $1/2^-$, while the theoretical cal- 378
 379 culations all give energies of the ground and first excited 380
 381 states very close to each other. At variance, the wider 382
 383 distributions (b) and (d) obtained for the 1340 keV tran- 384
 385 sition agreed well with an $\ell = 3$ angular momentum, 386
 387 consistent with the large spectroscopic factor and cross 388
 389 section calculated for the $7/2_1^-$ state in Table II. These 390

384 angular momentum assignments have also been tested 385
 386 with a Bayesian analysis [51]. We find that the \log_{10} 387
 388 scaled Bayes factors are always $\log_{10}(B_{10}) > 8$ ¹ such 389

¹ Bayes factors provide decisive evidence for one model when compared to another model if their $\log_{10}(B_{10})$ is larger than 2.

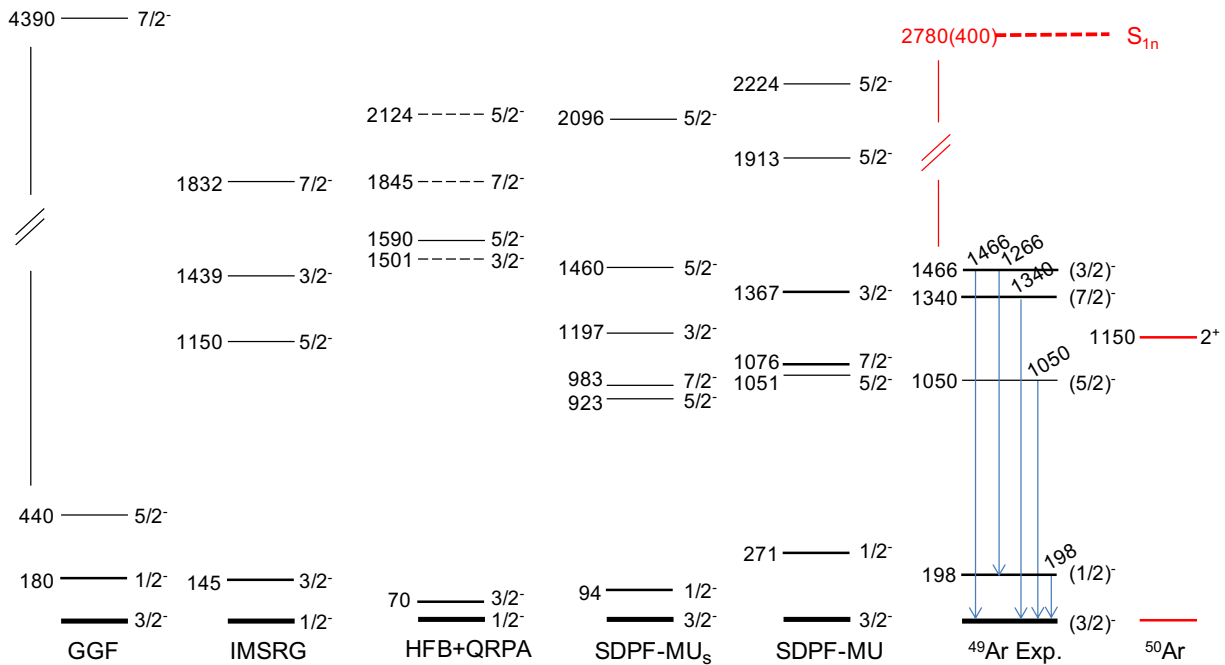


FIG. 5. Level scheme of ^{49}Ar with excitation energies expressed in keV. Experimental results (right) are obtained from the analyses of Fig. 2. They are compared to the theoretical calculations developed in the text: from right to left, shell-model calculations performed with the SDPF-MUs and the original SDPF-MU interactions, energy-density functional calculations including states obtained from QRPA (dashed lines), IMSRG calculation with the EM 1.8/2.0 interaction and GGF calculation with the $NN + 3N(\ln l)$ interaction; ^{50}Ar is shown on the right side with the latest $E(2_1^+)$ value taken from [29].

387 that a p -wave character is preferred over an f -wave in
 388 the 198 keV state distributions; in the 1340-keV state
 389 distributions, an f -wave over p -wave with $\log_{10}(B_{10}) >$
 390 6, which quantitatively supports the ℓ assignment.

391 For the ground state, we calculate momentum distribu-
 392 tions from the difference between the inclusive distribu-
 393 tion and the sum of contributions from the most intense
 394 transitions at 198 and 1340 keV due to the lack of statis-
 395 tics in each bin for other contributions. The resulting
 396 distributions do not allow to conclude between a pure
 397 $\ell = 1$ nor $\ell = 3$ character. However, as shown further,
 398 all theoretical calculations predict $\ell = 1$ for the ground
 399 state of ^{49}Ar .

400 D. Level scheme

401 Based on these observations, a tentative level scheme
 402 for ^{49}Ar is proposed in Fig. 5.

403 Except for the $\ell = 1$ value of the first excited state,
 404 there is no direct experimental information for the spin-
 405 parity assignment of the ground and first excited state.
 406 Compared to theoretical calculations, they are consistent
 407 with a spin-parity of either $1/2_1^-$ or $3/2_1^-$.

408 On the basis of momentum distributions, the most in-
 409 tense transition at 1340 keV is assigned to the decay
 410 of the $7/2^-$ state, either by $E2$ transition to $3/2^-$ or
 411 $E4(M3)$ to $1/2^-$. The prompt character of the observed

412 transition is in favor of a $E2$ transition. Since the inten-
 413 sity of the 1340 keV transition is much larger than the
 414 one of the 198 keV transition, we conclude for a direct
 415 decay by $E2$ transition from a level at 1340 keV to the
 416 $3/2_1^-$ ground state, as shown in Fig. 5. The first excited
 417 state at 198 keV is proposed to be of spin-parity $1/2_1^-$.

418 The 1466 keV transition is proposed to be a direct de-
 419 cay to the ground state from the $3/2_2^-$ state, present
 420 in theoretical calculations with a single particle char-
 421 acter. A decay to the first excited $1/2_1^-$ state is pro-
 422 posed through 1266 keV transition. The branching ratio
 423 obtained from the intensity ratio of the two transitions
 424 I_{1466}/I_{1266} is expected to be the same in the two differ-
 425 ent reaction channels, one neutron knockout and multi-
 426 nucleon removal. Due to the overwhelming transition at
 427 1340 keV, there is a strong uncertainty on the intensity
 428 of the transition at 1266 keV, which could partly explain
 429 the difference of 1.6(4) for the one neutron knockout and
 430 0.7(2) for the other channel, when the amplitude of re-
 431 sponse functions are free parameters of the fit. Alter-
 432 natively, a ratio fixed to 1.6 could also provides a good
 433 reproduction of Fig. 2 (b) with only a small increase of
 434 the χ^2 value. Unresolved small contributions - possibly
 435 coming from cascade decays of $5/2_2^-$ or $7/2_3^-$ - might also
 436 play a role that calls for a better gamma-ray energy res-
 437 olution.

438 For the last transition observed at 1050 keV, we have
 439 no strong experimental proposition, except that the the-

440 oretical calculations predict a $5/2_1^-$ state at nearby exci-
 441 tation energy and quite a small spectroscopic factor. It
 442 is consistent with a weak direct population in the one-
 443 neutron knockout, while it could be fed by unresolved
 444 high spin states populated in the multi-nucleon removal,
 445 such as the $5/2_2^-$ state.

446 E. Cross sections

447 Inclusive and exclusive cross sections have been calcu-
 448 lated using the same prescriptions detailed in Ref. [36].
 449 The only difference comes from the value of the effi-
 450 ciency for the detection of one proton in the MINOS
 451 setup $\varepsilon_{MINOS} = 0.71(2)$, which has been used here for
 452 the $^{50}\text{Ar}(p,pn)$ channel. This value is consistent with
 453 other (p,pn) analyses with the MINOS setup, such as
 454 in [16, 45].

455 Before subtraction, the contribution from the inelastic
 456 scattering channel $^{50}\text{Ar}(p,p')^{50}\text{Ar}$ decaying to ^{49}Ar was
 457 determined to be 4.8% of the total events, predominantly
 458 in the population of states leading to the 198 keV (6.4%),
 459 1050 keV (15.5%), and 1340 keV (3.9%) transitions.

460 Intensity values of 5.4(3), 1.5(3), 2.4(5), 8.3(7), and
 461 3.9(5) mb were determined for the 198, 1050, 1266, 1340,
 462 and 1466 keV transitions, respectively. According to the
 463 level scheme shown in Fig. 5, we obtained the experi-
 464 mental exclusive cross sections σ_{exp} for the direct popu-
 465 lation of states in the $^{50}\text{Ar}(p,pn)^{49}\text{Ar}$ knockout displayed
 466 in Tab. II.

467 Due to the Doppler shift, the transition at 198 keV
 468 spreads downwards in energy for detectors placed in the
 469 backward direction in the laboratory frame. The possi-
 470 ble impact of the energy threshold has been checked by
 471 selecting a set of detectors corresponding to the three
 472 first layers in the forward direction of DALI2⁺, as shown
 473 in Ref. [52]. The obtained cross sections are compared
 474 to values for the full ensemble of DALI2⁺: 5.39(33) and
 475 4.99(38) mb for the transition at 198 keV, respectively.
 476 The same was done for the transition at 1340 keV with
 477 8.26(66) and 7.39(72) mb. There is no evidence of an
 478 impact within the error bars and no difference with the
 479 1340 keV transition for which no impact is expected.

480 Experimental values are compared to the results of
 481 cross section calculations $\sigma_i^{ex}(E^*)$ for excitation energies
 482 E^* at a given incident energy E_{inc} following

$$\sigma_i^{ex}(E^*) = \sum_{l,j} C^2 S_{l,j}^i \cdot \sigma_{sp}^{lj}(E^*, E_{inc}) \quad (1)$$

483 where the theoretical spectroscopic factors $C^2 S_{l,j}^i$
 484 are multiplied by the single particle cross sections
 485 $\sigma_{sp}^{lj}(E^*, E_{inc})$ obtained in a reaction model. Here, they
 486 were calculated with the TC [47] and DWIA [48] meth-
 487 ods at 217 MeV/nucleon, which corresponds to the mid-
 488 target energy for ^{50}Ar projectiles. Values are given in
 489 Tab. II and used in the calculation of σ_{th} for the pre-
 490 dicted states below the one-neutron separation energy.

491 An overall agreement is observed with experimental val-
 492 ues, except for the large value predicted for the popula-
 493 tion of the $7/2_1^-$ state, which possibly suggests a smaller
 494 spectroscopic factor.

495 The inclusive cross section was determined to be σ_{inc}
 496 = 36.3(9) mb. The cross section to populate the ground
 497 state was calculated as the difference between the in-
 498 clusive cross section and the sum of the exclusive cross
 499 sections for transitions known to feed the ground state.
 500 This prescription is valid as long as the feeding from
 501 unresolved higher-lying states is negligible. This is a
 502 first-order approximation, reasonable considering the low
 503 value of the one-neutron separation energy S_n . However,
 504 in the list of higher-lying states predicted in the SDPF-
 505 MUs calculation, states such as $5/2_2^-$ or $7/2_3^-$ could
 506 partly populate the ground state with non-identified
 507 weak transitions. Therefore, the result of 17.2 mb has
 508 to be considered as an upper limit for σ_{gs} .

509 Overall consistency may be tested through the reduc-
 510 tion factor $R_s = \sigma_{inc} / \sum \sigma_{th,i}$, using the spectroscopic
 511 factor predictions of a shell model routinely used in this
 512 region like SDPF-MUs calculation in Tab. II. The value
 513 $R_s = 0.85(2)$ is found with the TC and DWIA reaction
 514 models, which places $^{50}\text{Ar}(p,pn)$ ($\Delta S = -17.8$ MeV) in
 515 the general trend observed for the one nucleon knockout
 516 reactions (see Ref. [53] and Fig.2 in Ref. [54]).

517 IV. DISCUSSION

518 In the following, the $N = 32$ neutron number is in-
 519 vestigated for ^{50}Ar , together with the reference nucleus
 520 ^{52}Ca . Properties of the even-even nuclei, as well as the
 521 $N - 1$ ones obtained from the one-neutron knockout, are
 522 discussed with the help of different theoretical methods.

523 First, shell-model calculations were performed using
 524 different versions of the SDPF-MU interaction, which
 525 were tuned to reproduce data in this mass region. Ad-
 526 ditional insight on excited states and the quadrupole
 527 deformation degree of freedom is then provided via
 528 Hartree-Fock-Bogoliubov (HFB) calculations based on
 529 the D1M parametrization [55] of the Gogny effective in-
 530 teraction [56]. Finally, new results from valence-space
 531 and full-space *ab initio* approaches are also provided to
 532 complete the theoretical analysis. Some of these theo-
 533 retical tools were already employed in Ref. [36], where
 534 details about the computational schemes can be found.

535 The computed low-lying spectra using these methods
 536 are displayed in Fig. 5. Other theoretical results are
 537 shown in Figs. 6-8, while numerical values are given in
 538 Tables III to VI in the text and in the Appendix.

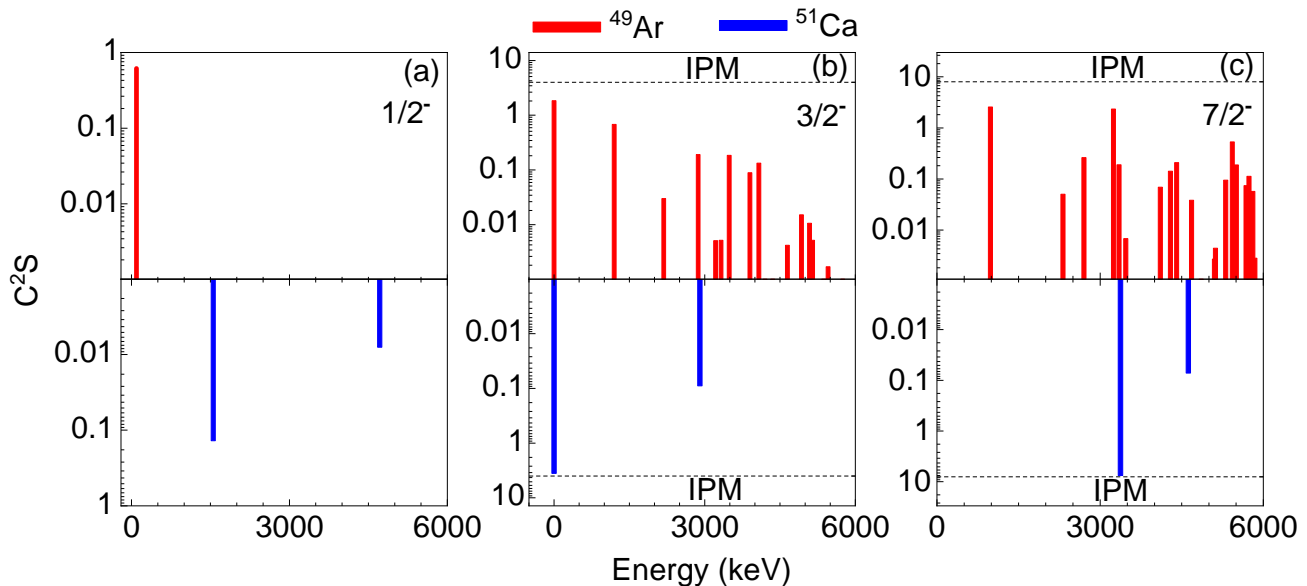


FIG. 6. Spectroscopic factor $\| \langle ^{A-1}X + n \mid ^A X \rangle \|^2$ distributions for (a) $1/2^-$, (b) $3/2^-$ and (c) $7/2^-$ states in ^{49}Ar (red) and ^{51}Ca (blue) obtained in the shell-model calculation with the SDPF-MUs interaction [46]. The dashed line corresponds to the maximal occupancy $2j + 1$ of the corresponding neutron orbitals $\nu 1p_{3/2}$ and $\nu 0f_{7/2}$ in an independent particle model (IPM).

TABLE III. Neutron content N_ν of the different fp orbitals in the gs wave function of ^{52}Ca and ^{50}Ar obtained in the shell-model calculation using the SDPF-MUs interaction.

$N_\nu(nlj)$	^{52}Ca	^{50}Ar
$\nu 0f_{7/2}$	7.95	7.61
$\nu 0f_{5/2}$	0.13	0.41
$\nu 1p_{3/2}$	3.76	3.28
$\nu 1p_{1/2}$	0.17	0.70

TABLE IV. $0p0h$ and $2p2h$ components of the wave function for the lowest two 0^+ of ^{52}Ca and ^{50}Ar , obtained in the shell-model calculation using the SDPF-MU interaction.

	Energy (keV)	$0p0h$ %	$2p2h$ %
$^{52}\text{Ca } 0_1^+$	gs	87.1	12.4
$^{52}\text{Ca } 0_2^+$	4007	7.3	88.9
$^{50}\text{Ar } 0_1^+$	gs	54.0	28.8
$^{50}\text{Ar } 0_2^+$	2412	25.4	58.5

A. Shell-model calculations

The shell-model calculations were performed with the SDPF-MUs interaction, which was derived from the original SDPF-MU interaction [57] and tuned to improve the results for K and Ca isotopes [46]. This tuning was useful to reproduce the excitation energy of the first 2^+ state in argon isotopes up to ^{52}Ar [27]. However, the level

scheme in Fig.5 is better reproduced with the original SDPF-MU interaction. A slightly larger compression is observed with SDPF-MUs, with nevertheless the same level ordering.

In a shell-model picture, one would expect, for a closed-shell nucleus at $N = 32$ in a spherical configuration, the $\nu 0f_{7/2}$ and $\nu 1p_{3/2}$ orbitals to be filled and $\nu 1p_{1/2}$ and $\nu 0f_{5/2}$ orbitals to be empty. The numerical values for the neutron content N_ν of the ^{52}Ca and ^{50}Ar orbitals are displayed in Tab. III. The $\nu 1p_{3/2}$ and $\nu 0f_{7/2}$ orbitals are slightly emptied in ^{50}Ar compared to the closed shell isotope ^{52}Ca , with a corresponding increase for the $\nu 1p_{1/2}$ and $\nu 0f_{5/2}$ orbitals. The relative effect is quite strong for $\nu 1p_{1/2}$. This change is not driven by the monopole gap between the $\nu 1p_{3/2}$ and $\nu 1p_{1/2}$ orbitals which do not significantly change from one nucleus to the other, as already mentioned in Ref. [28]. At the same time, more mixing is predicted in Tab. IV for the wave function of the ^{50}Ar ground state, compared to ^{52}Ca . The SDPF-MU calculation in Ref. [29] also predicts for ^{50}Ar a ratio $E(4_1^+)/E(2_1^+) = 2.05$, consistent with a vibrational character. This is the first indication of collective effects present in ^{50}Ar .

The one neutron knockout $^{50}\text{Ar}(p,pn)$ is a good tool to test the persistence of the shell effect observed at $N = 32$ on ^{52}Ca , as recently obtained for $^{52}\text{Ca}(p,pn)$ [16]. Without correlations, the occupancy number should be found at $2j + 1$ for fully-occupied orbitals and 0 for empty ones. The spectroscopic factor C^2S distributions calculated for the low-lying $1/2^-$, $3/2^-$ and $7/2^-$ states in ^{49}Ar and ^{51}Ca are shown in Fig.6.

$3/2^-$ states

580 The C^2S value for the $3/2_1^-$ ground state in ^{51}Ca is
 581 very close to the $2j + 1$ value, which is a signature of
 582 a single-particle character with a strong overlap with a
 583 neutron hole in the $\nu 1p_{3/2}$ orbital in ^{52}Ca . In ^{49}Ar and
 584 in spite of the high excitation energy range, the sum
 585 $\sum_i (C^2S)_i = 3.19$ is still lower than the value for $3/2_1^-$ in
 586 ^{51}Ca , with evidence for a fragmentation of the distribution.
 587 The shell model calculation predicts a $3/2_1^-$ ground
 588 state for ^{49}Ar . It also predicts a $3/2_2^-$ state at 1197 keV
 589 with a significant spectroscopic factor, which we assume
 590 to be consistent with the 1466 keV state in Fig. 5 and
 591 the measured cross sections. Higher-lying states are also
 592 predicted, such as $3/2_4^-$ at 2870 keV very close to the
 593 estimated S_n value. If not unbound, they will be part of
 594 the feeding to lower-lying states.

595 $1/2^-$ states

596 The $1/2_1^-$ state in ^{51}Ca has a large excitation energy at
 597 about 1.5 MeV and a small spectroscopic factor. This is
 598 consistent with a weak population of the $\nu 1p_{1/2}$ orbital
 599 in ^{52}Ca , such as the removal of a $1p_{1/2}$ neutron from
 600 a $(\nu 1p_{3/2})^2(\nu 1p_{1/2})^2$ configuration with a small weight
 601 in the ^{52}Ca wave function and a large $\nu 1p_{3/2} - \nu 1p_{1/2}$
 602 spherical gap. This is what is expected for a closed shell
 603 nucleus at $N = 32$ in the shell model framework. A very
 604 different conclusion may be drawn for ^{49}Ar . The energy
 605 difference between the ground and the first excited state
 606 is found to be quite small in many calculations. The
 607 shell model calculation with the SDPF-MUs interaction
 608 predicts the $1/2_1^-$ state at 94 keV. A comparably small
 609 value is obtained with the original SDPF-MU interaction.
 610 Whereas the C^2S value for $3/2_1^-$, although large, is
 611 well reduced compared to the ^{51}Ca case, the C^2S value
 612 for $1/2_1^-$ significantly increases from ^{51}Ca to ^{49}Ar . The
 613 experimental cross section measured for the first excited
 614 state in ^{49}Ar , assumed to be $1/2_1^-$, is consistent with the
 615 large value C^2S calculated with the SDPF-MUs interaction
 616 in Tab. II. Both the low excitation energy and the
 617 substantial C^2S value of the $1/2_1^-$ state are clear indica-
 618 tions of collective effects present in ^{49}Ar .

619 $5/2^-$ states

620 A $5/2_1^-$ state is found in most of the calculations
 621 around 1 MeV, which supports the assumption of such a
 622 state at 1050 keV in Fig. 5. It is weakly populated in the
 623 neutron knockout reaction, as expected from the small
 624 value of the spectroscopic factor displayed in Tab. V. A
 625 large value $B(E2; 5/2_1^- \rightarrow 1/2_1^-) = 177 e^2 fm^4$ is also
 626 predicted.

627 $7/2^-$ states

628 Here again ^{51}Ca and ^{49}Ar are found to be quite
 629 different. There is mainly one low-lying $7/2^-$ state
 630 in ^{51}Ca , around 3 MeV with a large C^2S value, very
 631 close to the $2j + 1$ limit in Fig. 6 (c). This strong
 632 overlap is consistent with a neutron hole in the $\nu 0f_{7/2}$
 633 orbital in ^{52}Ca . In ^{49}Ar , in spite of the high excitation
 634 energy range, the sum $\sum_i (C^2S)_i = 6.95$ is still lower
 635 than the value for $7/2_1^-$ in ^{51}Ca , with evidence for a
 636 fragmentation of the distribution. Two states, $7/2_1^-$
 637 and $7/2_4^-$, have a large C^2S value. The origin of the

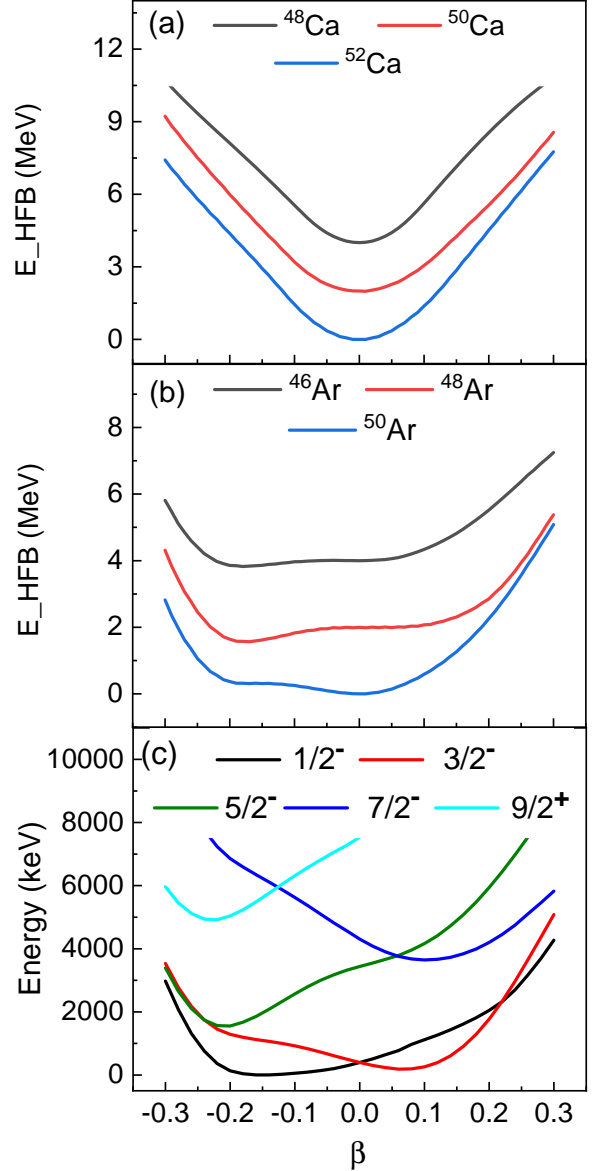


FIG. 7. Potential energy surfaces energy E_{HFB} versus the quadrupole deformation parameter β for argon a) and calcium b) isotopes obtained from HFB calculations based on the DIM parametrisation [55] of the Gogny effective interaction [56]. The curves are shifted by 2 MeV from each other in order to allow superposition; (c) HFB + blocking calculations (see text) for the lowest-lying states of ^{49}Ar at a given spin-parity $1/2^-, 3/2^-, 5/2^-, 7/2^-$ and $9/2^+$.

638 calculated $7/2_4^-$ state can be easily understood since
 639 its excitation energy is predicted to be 3245 keV, very
 640 similar to the value obtained for $7/2_1^-$ in ^{51}Ca . It can
 641 therefore be associated with the neutron removal from
 642 the spherical $\nu 0f_{7/2}$ orbital. The excitation energy of
 643 such a state is well above the one-neutron separation
 644 energy S_n . This calls for invariant mass reconstruction,

645 which will not be discussed here.

646
647 The $7/2_1^-$ state seems more complex, with a low
648 excitation energy $E^* = 983$ keV and a large value
649 $B(E2; 7/2_1^- \rightarrow 3/2_1^-) = 144.2 e^2 fm^4$ to the ground state.
650 In the shell-model framework, it is tempting to link it
651 with a more complex neutron configuration in ^{50}Ar , in-
652 volving some $\nu(1p_{3/2})^2(1p_{1/2})^2$ components compared to
653 $\nu(1p_{3/2})^4$, already encountered for the population of the
654 $1/2_1^-$ state. Its energy is also close to the 2_1^+ state exci-
655 tation energy in ^{50}Ar , which suggests a vibrational com-
656 ponent for a state built on the $3/2_1^-$ ground state.

657 With small C^2S values, the $7/2_2^-$ and $7/2_3^-$ states are
658 weakly populated in the one-neutron knock-out. More-
659 over, they do not directly decay to the ground state, feed-
660 ing states at lower excitation energy in a complex decay
661 pattern.

662 B. Energy-density functional calculations

663 The analysis is complemented with results of energy-
664 density functional calculations based on the D1M
665 parametrization [55] of the Gogny effective interac-
666 tion [56]. The potential energy surfaces (PES) are shown
667 in Fig. 7 for calcium and argon isotopes. While the cal-
668 cium isotopes are found to be spherical, PES are much
669 softer for argon isotopes and a trend towards oblate de-
670 formation is observed, favored by the gain in energy
671 for the $3/2^+[202]$ proton orbital, as observed in Fig. 8
672 (left panel). This results in a competition between the
673 spherical minimum and an oblate configuration around
674 $\beta \simeq -0.2$. At the mean-field level, permanent oblate de-
675 formation is predicted for ^{48}Ar , but ^{50}Ar remains spher-
676 ical.

677 In the present HFB calculations assuming axial sym-
678 metry around the z-axis, the low-lying states in ^{49}Ar
679 are described within the blocking approximation by a
680 one-quasiparticle (qp) excitation on top of a qp vacuum.
681 Along the binding energy minimization process, the occu-
682 pation probability of the one-qp orbital is imposed.
683 This orbital is selected according to its quantum num-
684 bers and numbering by its qp energy, i.e., with respect to
685 the Fermi level. Odd-A HFB states with spin-parity J^π
686 are obtained by selecting qp orbitals with angular mo-
687 mentum projection and parity $K^\pi = J^\pi$. On top of the
688 HFB with K blocking calculations, vibrational states are
689 described within a consistent QRPA approach. More de-
690 tails can be found concerning the HFB and HFB+QRPA
691 approaches in Refs. [58, 59] for the treatment of odd sys-
692 tems. The minimization of the lowest energy states with
693 parity $1/2^-$ to $7/2^-$ and $9/2^+$ versus the quadrupole de-
694 formation is shown in Fig. 7.

695 The D1M mean-field ground state is obtained by block-
696 ing on the first $K=1/2$ quasi-particle orbital, with a soft
697 oblate minimum at $\beta = -0.15$. It is consistent with
698 the neutron knockout from the valence orbital $1/2^- [321]$
699 in ^{50}Ar at moderate oblate deformation. Here again,

700 the $1/2_1^-$ and $3/2_1^-$ states are very close to each other,
701 but $3/2_1^-$ is found as nearly spherical excited state at 70
702 keV. The next $3/2^-$ state is found by blocking at much
703 higher energy around 3350 keV. Therefore, the experi-
704 mental $3/2_2^-$ state at 1466 keV seems to be more consis-
705 tent with a collective state, at about the same energy as
706 the 2_1^+ state in ^{50}Ar .

707 Blocking the first $K = 5/2$ qp orbital, the $5/2_1^-$ state
708 is found at 1590 keV above the $1/2^-$ HFB minimum and
709 an oblate deformation $\beta = -0.20$. It is partly associ-
710 ated to the $K=5/2$ orbital of $\nu 0f_{5/2}$ parentage, $5/2^- [303]$
711 in Fig. 8 (right panel), which is strongly favored by the
712 oblate deformation. Another origin could be a collective
713 state, such as a vibrational $K = 2$ state built on top of
714 the $1/2_1^-$ state.

715 Blocking the $K=7/2$ qp orbital, no $7/2^-$ state is ob-
716 tained below 3 MeV. The first $7/2^-$ state is found at
717 3650 keV with a small prolate deformation $\beta_2 = +0.1$.
718 It is closely related to the $7/2^- [303]$ orbital, with a
719 nearly pure wave function. This suggests that the ex-
720 perimental $7/2_1^-$ state at 1340 keV in Fig. 5 could partly
721 be a vibrational one. From QRPA calculations per-
722 formed for phonons acting on the odd QRPA ground
723 state $J = 3/2^-$, the experimental state might be a mix-
724 ing of the three QRPA states obtained for the $K = 0$,
725 1 and 2 phonons, the main component being the QRPA
726 state for the $K = 0$ at 1775 keV.

727 This discussion, based on shell model calculations as
728 well as an energy-density functional approach, is consis-
729 tent with a sharp transition from a spherical configura-
730 tion at $N = 32$ when protons are removed from ^{52}Ca
731 to ^{50}Ar . A low-lying $1/2^-$ state in ^{49}Ar , as well as $7/2^-$
732 and $3/2^-$ states at excitation energies close to the first 2_1^+
733 state in ^{50}Ar , may be assigned to the existence of collec-
734 tive effects. This evolution is now also been investigated
735 with the help of recently developed *ab initio* approaches.

736 C. *Ab initio* calculations

737 *Ab initio* calculations were performed in the context of
738 the valence-space in-medium similarity renormalization
739 group (VS-IMSRG) [60] and the self-consistent Gorkov
740 Green's function (GGF) [61, 62] approaches.

741 In the VS-IMSRG approach, the *sd* and the full
742 *pf* shells above a ^{28}O core were considered for proton
743 and neutron valence spaces, respectively. Three-nucleon
744 forces between valence nucleons were captured via en-
745 semble normal ordering [63]. Calculations were per-
746 formed within 15 major oscillator shells, whereas an ad-
747 ditional cut on three-nucleon configurations was intro-
748 duced at $E_{3\max} = 24$ [64]. The spectroscopic factors
749 were computed with the bare annihilation operators, al-
750 though ideally, they should be evolved consistently with
751 the Hamiltonian. The consistent evolution would change
752 the spectroscopic factor by roughly 10% [65]. The two

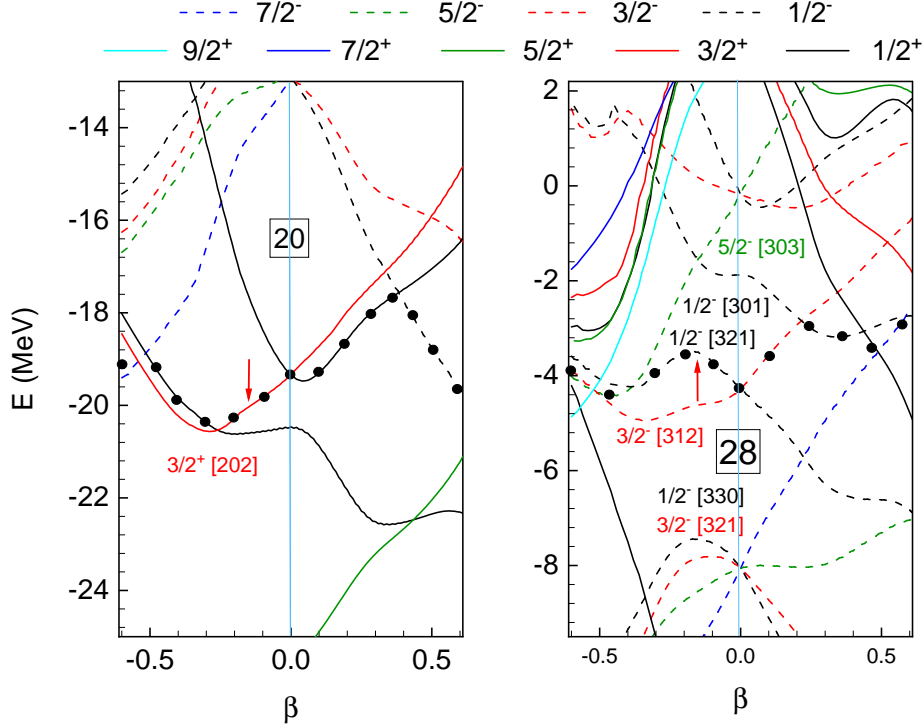


FIG. 8. Energy of the proton (left) and neutron (right) orbitals versus the quadrupole deformation β parameter in ^{50}Ar obtained from Hartree-Fock-Bogoliubov (HFB) calculations based on the D1M parametrisation [55] of the Gogny effective interaction [56]. The orbitals discussed in the text are labeled with the usual Nilsson parameters $K[N, n_z, \Lambda]$. The black dots stand for the Fermi level. The red arrow is placed at $\beta = -0.15$.

753 plus three-nucleon $1.8/2.0$ EM interaction [66] was em-
 754 ployed throughout the study.

755 VS-IMSRG predictions for low-lying states are similar
 756 to the ones from the SDPF-MUs calculation, with two
 757 main exceptions. First, a less compressed level scheme is
 758 found for ^{49}Ar , as visible from Fig. 5. Moreover, a spin
 759 inversion for the ground state ($1/2^-$ instead of $3/2^-$) is
 760 predicted, although the two states are very close to each
 761 other in excitation energy. This spin inversion is also ob-
 762 served in VS-IMSRG calculations performed with other
 763 interactions, such as $\Delta\text{NNLO}_{\text{GO}}$ [67] or $\text{NN}+3\text{N}(\text{lnl})$ [68].

764 GGF calculations were performed in the A -body
 765 Hilbert space truncated to 14 major oscillator shells,
 766 with a further cut on three-nucleon matrix elements im-
 767 posed by $E_{3\text{max}} = 16$. Although the latter is smaller
 768 than the one introduced in VS-IMSRG calculations, it is
 769 sufficient to converge all relevant observables. Two dif-
 770 ferent interactions were employed, namely NNLO_{sat} [69]
 771 and $\text{NN} + 3\text{N}(\text{lnl})$ [68]. As for the other theoretical ap-
 772 proaches, the properties of the low-lying states in ^{51}Ca
 773 suggest that ^{52}Ca is a closed-shell nucleus: *i*) large C^2S
 774 values close to the $2j + 1$ limit for the $3/2^-$ ground state
 775 and $7/2^-$ fragment found at high excitation energy for
 776 both interactions; *ii*) the first $1/2^-$ state appears at high
 777 excitation energy, especially with NNLO_{sat} , and has very

778 small C^2S values.

779 In contrast, corresponding results for ^{49}Ar point to the
 780 emergence of a qualitatively different picture. The C^2S
 781 values for the main $3/2^-$ and $7/2^-$ states decrease, al-
 782 though the change is quantitatively different with the two
 783 interactions. While the reduction is significant (around
 784 30%) for $\text{NN} + 3\text{N}(\text{lnl})$, only a $\sim 5 - 10\%$ decrease is ob-
 785 served for NNLO_{sat} . This is presumably due to the fact
 786 that the former interaction predicts consistently smaller
 787 $0d_{3/2} - 1s_{1/2}$ proton gaps, hence favoring more fragmen-
 788 tation in spite of being sensibly more perturbative of
 789 NNLO_{sat} . Contrarily to valence-space calculations, here,
 790 the energy of the $7/2^-$ state changes by only a few hun-
 791 dred keV, and a component below 1 MeV is not observed
 792 for this angular momentum. Importantly, together with
 793 the reduction of spectroscopic factors, a low-energy $1/2^-$
 794 state appears with both interactions. In addition, the
 795 energy of the first $5/2^-$ state is lowered by more than 1
 796 MeV. These features all signal an increase of collectivity
 797 in ^{49}Ar .

798 Altogether, the changes observed in GGF calculations
 799 when going from ^{51}Ca to ^{49}Ar are consistent with shell
 800 model results and point to the deterioration of the $N =$
 801 32 gap in argon. The quantitative differences emerging in
 802 the two sets of results are very likely due to the missing

collective degrees of freedom (i.e., lack of deformation and low truncation in the particle-hole expansion) in the GGF approach.

V. CONCLUSIONS

In summary, the one neutron knock-out $^{50}\text{Ar}(p,pn)$ reaction was studied in inverse kinematics on a thick liquid hydrogen target at about 217 MeV/u. The spectroscopy of ^{49}Ar was obtained by fast in-beam γ -ray measurements with the help of the DALI2⁺ array for transitions from low-lying bound states. A first level scheme could be proposed for ^{49}Ar , with tentative assignment of spin parities for the $1/2_1^-$ and $7/2_1^-$ excited states.

The resulting low-energy spectroscopy of ^{49}Ar and cross sections, in addition to the spectroscopic factors obtained in theoretical calculations, are consistent with a description more complex than that used for ^{51}Ca , as illustrated by the PES in HFB calculations. While a spherical configuration, expected from the $N = 32$ shell closure, is still present in ^{49}Ar for some states (such as the $3/2_1^-$ ground state or the $7/2_4^-$ state in the SDPF-MUs calculation), one also observes the onset of collective effects consistent with quadrupolar deformation or vibration. In particular, this is manifested by the low excitation energy and substantial C^2S values of the $1/2_1^-$ state. Interestingly, this collective character is not driven by a reduction of the $N = 32$ gap, which roughly remains constant when going from calcium to argon. *Ab initio* calculations also consistently predict an increase of collectivity in ^{49}Ar as compared to ^{51}Ca . This is indicated by the appearance of low-energy states in the excitation spectrum as well as a significantly more fragmented strength in argon. In the future, it will be interesting to further investigate these findings in the ^{48}S isotone, for which the proton valence orbital from $\pi 1s_{1/2}$ parentage has a very different dependence on quadrupole deformation.

VI. APPENDIX

Tab. V and VI are displayed the numerical values of the excitation energies and spectroscopic factors for the states populated in the one-neutron knockout from ^{50}Ar and ^{52}Ca obtained in the theoretical calculations given in the main text.

ACKNOWLEDGMENTS

We thank the RIKEN Nishina Center accelerator staff for their work in the primary beam delivery and the BigRIPS team for preparing the secondary beams. The

development of MINOS has been supported by the European Research Council through the ERC Grant No. MINOS258567. B. D. L. and L. X. C. acknowledge support from the Vietnam Ministry of Science and Technology under Grant No. ĐTCB.01/21/VKHKTHN. M.G.-R. and A.M.M. acknowledge financial support by MCIN/AEI/10.13039/501100011033 under I+D+i project No. PID2020-114687GB-I00 and under grant IJC2020-043878-I (also funded by “European Union NextGenerationEU/PRTR”), by the Consejería de Economía, Conocimiento, Empresas y Universidad, Junta de Andalucía (Spain) and “ERDF-A Way of Making Europe” under PAIDI 2020 project No. P20_01247, and by the European Social Fund and Junta de Andalucía (PAIDI 2020) under grant number DOC-01006. T. M. acknowledges the European Research Council (ERC) under the European Union’s Horizon 2020 research and innovation programme (grant agreement No 101020842) F.B. was supported by the RIKEN Special Postdoctoral Researcher Program. Y. L. S. acknowledges the support of Marie Skłodowska-Curie Individual Fellowship (H2020-MSCAIF-2015-705023) from the European Union. I. G. has been supported by HIC and Croatian Science Foundation. R. -B. G. is supported by the Deutsche Forschungsgemeinschaft (DFG) under Grant No. BL 1513/1-1. K. I. H., D. K., and S. Y. P. acknowledge the support from the IBS grant funded by the Korea government (No. IBS-R031-D1). P. K. and V. W. were supported in part by the BMBF grants No. 05P19RDFN1, 05P21RDFN1 and HGS-HIRE. D. So. has been supported by the National Research, Development and Innovation Fund of Hungary via Project No. K128947 and TKP2021-NKTA-42. P. -A. S. acknowledges the support from BMBF under grant NuSTAR.DA 05P15RDFN1 and contract PN 23.21.01.06 sponsored by the Romanian Ministry of Research, Innovation and Digitalization. This work was supported in part by JSPS KAKENHI Grants No. JP16H02179, JP18H05404 and JP20K03981. J. D. H. acknowledges the support from NSERC, the National Research Council Canada, and the Arthur B. McDonald Canadian Astroparticle Physics Research Institute. T. M. acknowledges the support from the Deutsche Forschungsgemeinschaft (DFG, German Research Foundation) – Project-ID 279384907 – SFB 1245. This work was supported by the Office of Nuclear Physics, U.S. Department of Energy, under Grants No. de-sc0018223 (NUCLEI SciDAC-4 collaboration) and the FieldWork Proposal ERKBP72 at Oak Ridge National Laboratory (ORNL). Computer time was provided by the Innovative and Novel Computational Impact on Theory and Experiment (INCITE) program. This research used resources of the Oak Ridge Leadership Computing Facility located at ORNL, which is supported by the Office of Science of the Department of Energy under Contract No. DE-AC05-00OR22725. GGF calculations were performed by using HPC resources from GENCI-TGCC (Contracts No. A0090507392, A0110513012) and at the DiRAC DiAL system at the University of

TABLE V. Spin J^π , excitation energies E^* and spectroscopic factors $\|\langle^{A+1}X - n \|^A X\rangle\|^2$ for levels of ^{49}Ar and ^{51}Ca obtained in shell-model calculation with the SDPF-MUs interaction and VS-IMSRG calculation with the 1.8/2.0 (EM) interaction [66].

State	SM (SDPF-MUs)				VS-IMSRG (1.8/2.0 EM)			
	^{49}Ar		^{51}Ca		^{49}Ar		^{51}Ca	
	E^* (keV)	C^2S	E^* (keV)	C^2S	E^* (keV)	C^2S	E^* (keV)	C^2S
$3/2_1^-$	gs	1.84	gs	3.57	155	1.37	gs	3.69
$1/2_1^-$	94	0.62	1552	0.14	gs	0.94	2025	0.09
$5/2_1^-$	923	<0.01	2298	<0.01	1150	<0.01	2068	0.00
$7/2_1^-$	983	2.56	3374	7.56	1852	1.89	4197	7.59
$3/2_2^-$	1197	0.68	2893	0.09	1439	0.91	3081	0.06
$7/2_2^-$	2317	0.05	4622	0.07	3271	0.09		

TABLE VI. Spin J^π , excitation energies E^* and spectroscopic factors $\|\langle^{A+1}X - n \|^A X\rangle\|^2$ for levels of ^{49}Ar and ^{51}Ca obtained in GGF calculations with the $NN + 3N(\text{lnl})$ and NNLO_{sat} interactions. Here we select states for which the spectroscopic factor is larger than 0.01.

State	GGF ($NN + 3N(\text{lnl})$)				GGF (NNLO_{sat})			
	^{49}Ar		^{51}Ca		^{49}Ar		^{51}Ca	
	E^* (keV)	C^2S	E^* (keV)	C^2S	E^* (keV)	C^2S	E^* (keV)	C^2S
$3/2^-$	gs	2.68	gs	3.36	gs	3.17	gs	3.34
$1/2^-$	180	0.22	1610	<0.01	330	0.02	3060	0.03
$5/2^-$	440	0.10	1628	<0.01	1890	<0.01	2980	<0.01
$7/2^-$	3590	0.10	3020	0.02	2480	0.48	4152	0.02
$3/2^-$	3620	0.01	1740	0.02	2690	0.02	3010	0.03
$7/2^-$	4390	3.64	3720	6.75	3980	5.59	4660	6.05

908 Leicester (funded by the UK BEIS via STFC Capital
909 Grants No. ST/K000373/1 and No. ST/R002363/1 and
910 STFC DiRAC Operations Grant No. ST/R001014/1)
911 and at the National Energy Research Scientific Com-
912 puting Center (NERSC), a U.S. Department of En-
913 ergy User Facility using awards NP-ERCAP0020946 and
914 NP-ERCAP0024959. This work was supported by the
915 United Kingdom Science and Technology Facilities Coun-
916 cil (STFC) under Grant No. ST/L005816/1 and in part
917 by the NSERC Grant Nos. SAPIN-2016-00033, SAPIN-
918 2018-00027, and RGPAS-2018-522453. TRIUMF re-
919 ceives federal funding via a contribution agreement with
920 the National Research Council of Canada. J. D. H., B.

921 S. H., and T. M. thanks S. R. Stroberg for the `imsrg++`
922 code used to perform the VS-IMSRG calculations [70].
923 The valence-space diagonalization of the VS-IMSRG cal-
924 culations were done with the `KSHELL` code [71]. The
925 VS-IMSRG computations were performed with an allo-
926 cation of computing resources on Cedar at WestGrid and
927 Compute Canada, and on the Oak Cluster at TRIUMF
928 managed by the University of British Columbia depart-
929 ment of Advanced Research Computing (ARC). N.T.T.P
930 is funded by the University of Science, VNU-HCM under
931 grant number T2021-02.

932 [1] O. Sorlin and M.-G. Porquet, *Physica Scripta* **T152**,
933 014003 (2013).
934 [2] B. Bastin, S. Grévy, D. Sohler, O. Sorlin, Z. Dom-
935 brádi, N. L. Achouri, J. C. Angélique, F. Azaiez, D. Bai-
936 borodin, R. Borcea, C. Bourgeois, A. Buta, A. Bürger,
937 R. Chapman, J. C. Dalouzy, Z. Dlouhy, A. Drouard,
938 Z. Elekes, S. Franchoo, S. Iacob, B. Laurent, M. Lazar,
939 X. Liang, E. Liénard, J. Mrazek, L. Nalpas, F. Negoita,
940 N. A. Orr, Y. Penionzhkevich, Z. Podolyák, F. Pougheon,

941 P. Roussel-Chomaz, M. G. Saint-Laurent, M. Stanoiu,
942 I. Stefan, F. Nowacki, and A. Poves, *Phys. Rev. Lett.*
943 **99**, 022503 (2007).
944 [3] S. Takeuchi, M. Matsushita, N. Aoi, P. Doornenbal,
945 K. Li, T. Motobayashi, H. Scheit, D. Steppenbeck,
946 H. Wang, H. Baba, D. Bazin, L. Căceres, H. Crawford,
947 P. Fallon, R. Gernhäuser, J. Gibelin, S. Go, S. Grévy,
948 C. Hinke, C. R. Hoffman, R. Hughes, E. Ideguchi,
949 D. Jenkins, N. Kobayashi, Y. Kondo, R. Krücken,

- T. Le Bleis, J. Lee, G. Lee, A. Matta, S. Michimasa, T. Nakamura, S. Ota, M. Petri, T. Sako, H. Sakurai, S. Shimoura, K. Steiger, K. Takahashi, M. Takeuchi, Y. Togano, R. Winkler, and K. Yoneda, *Phys. Rev. Lett.* **109**, 182501 (2012).
- [4] A. Gade, B. A. Brown, J. A. Tostevin, D. Bazin, P. C. Bender, C. M. Campbell, H. L. Crawford, B. Elman, K. W. Kemper, B. Longfellow, E. Lunderberg, D. Rhodes, and D. Weisshaar, *Phys. Rev. Lett.* **122**, 222501 (2019).
- [5] H. L. Crawford, P. Fallon, A. O. Macchiavelli, P. Doornenbal, N. Aoi, F. Browne, C. M. Campbell, S. Chen, R. M. Clark, M. L. Cortés, M. Cromaz, E. Ideguchi, M. D. Jones, R. Kanungo, M. MacCormick, S. Momiyama, I. Murray, M. Niikura, S. Paschalis, M. Petri, H. Sakurai, M. Salathe, P. Schrock, D. Steppenbeck, S. Takeuchi, Y. K. Tanaka, R. Taniuchi, H. Wang, and K. Wimmer, *Phys. Rev. Lett.* **122**, 052501 (2019).
- [6] T. Otsuka, R. Fujimoto, Y. Utsuno, B. A. Brown, M. Honma, and T. Mizusaki, *Phys. Rev. Lett.* **87**, 082502 (2001).
- [7] F. Wienholtz, D. Beck, K. Blaum, C. Borgmann, M. Breitenfeldt, R. B. Cakirli, S. George, F. Herfurth, J. D. Holt, M. Kowalska, S. Kreim, D. Lunney, V. Manea, J. Menéndez, D. Neidherr, M. Rosenbusch, L. Schweikhard, A. Schwenk, J. Simonis, J. Stanja, R. N. Wolf, and K. Zuber, *Nature* **498**, 346 (2013).
- [8] S. Michimasa, M. Kobayashi, Y. Kiyokawa, S. Ota, D. S. Ahn, H. Baba, G. P. A. Berg, M. Dozono, N. Fukuda, T. Furuno, E. Ideguchi, N. Inabe, T. Kawabata, S. Kawase, K. Kisamori, K. Kobayashi, T. Kubo, Y. Kubota, C. S. Lee, M. Matsushita, H. Miya, A. Mizukami, H. Nagakura, D. Nishimura, H. Oikawa, H. Sakai, Y. Shimizu, A. Stolz, H. Suzuki, M. Takaki, H. Takeda, S. Takeuchi, H. Tokieda, T. Uesaka, K. Yako, Y. Yamaguchi, Y. Yanagisawa, R. Yokoyama, K. Yoshida, and S. Shimoura, *Phys. Rev. Lett.* **121**, 022506 (2018).
- [9] W. S. Porter, E. Dunling, E. Leistenschneider, J. Bergmann, G. Bollen, T. Dickel, K. A. Dietrich, A. Hamaker, Z. Hockenbery, C. Izzo, A. Jacobs, A. Javaji, B. Kootte, Y. Lan, I. Miskum, I. Mukul, T. Murböck, S. F. Paul, W. R. Plaß, D. Puentes, M. Redshaw, M. P. Reiter, R. Ringle, J. Ringuette, R. Sandler, C. Scheidenberger, R. Silwal, R. Simpson, C. S. Sumithrarachchi, A. Teigelhöfer, A. A. Valverde, R. Weil, I. T. Yandow, J. Dilling, and A. A. Kwiatkowski, *Phys. Rev. C* **106**, 024312 (2022).
- [10] A. Huck, G. Klotz, A. Knipper, C. Miché, C. Richard-Serre, G. Walter, A. Poves, H. L. Ravn, and G. Marguier, *Phys. Rev. C* **31**, 2226 (1985).
- [11] A. Gade, B. A. Brown, D. Bazin, C. M. Campbell, J. A. Church, D. C. Dinca, J. Enders, T. Glasmacher, M. Horoi, Z. Hu, K. W. Kemper, W. F. Mueller, T. Otsuka, L. A. Riley, B. T. Roeder, T. Suzuki, J. R. Terry, K. L. Yurkewicz, and H. Zwahlen, *Phys. Rev. C* **74**, 034322 (2006).
- [12] S. Chen, F. Browne, P. Doornenbal, J. Lee, A. Obertelli, Y. Tsunoda, T. Otsuka, Y. Chazono, G. Hagen, J. D. Holt, G. R. Jansen, K. Ogata, N. Shimizu, Y. Utsuno, K. Yoshida, N. L. Achouri, H. Baba, D. Calvet, F. Château, N. Chiga, A. Corsi, M. L. Cortés, A. Delbart, J.-M. Gheller, A. Giganon, A. Gillibert, C. Hilaire, T. Isobe, T. Kobayashi, Y. Kubota, V. Lapoux, T. Motobayashi, I. Murray, H. Otsu, V. Panin, N. Paul, W. Rodriguez, H. Sakurai, M. Sasano, D. Steppenbeck, L. Stuhl, Y. L. Sun, Y. Togano, T. Uesaka, K. Wimmer, K. Yoneda, O. Aktas, T. Aumann, L. X. Chung, F. Flavigny, S. Franchoo, I. Gasparic, R.-B. Gerst, J. Gibelin, K. I. Hahn, D. Kim, Y. Kondo, P. Koseoglou, J. Lee, C. Lehr, P. J. Li, B. D. Linh, T. Lokotko, M. MacCormick, K. Moschner, T. Nakamura, S. Y. Park, D. Rossi, E. Sahin, P.-A. Söderström, D. Sohler, S. Takeuchi, H. Toernqvist, V. Vaquero, V. Wagner, S. Wang, V. Werner, X. Xu, H. Yamada, D. Yan, Z. Yang, M. Yasuda, and L. Zanetti, *Phys. Lett. B* **xx**, xx (2023), accepted.
- [13] H. Scheit, T. Glasmacher, B. A. Brown, J. A. Brown, P. D. Cottle, P. G. Hansen, R. Harkewicz, M. Hellström, R. W. Ibbotson, J. K. Jewell, K. W. Kemper, D. J. Morrissey, M. Steiner, P. Thirolf, and M. Thoennessen, *Phys. Rev. Lett.* **77**, 3967 (1996).
- [14] S. Calinescu, L. Cáceres, S. Grévy, O. Sorlin, Z. Dombrádi, M. Stanoiu, R. Astabatyán, C. Borcea, R. Borcea, M. Bowry, W. Catford, E. Clément, S. Franchoo, R. Garcia, R. Gillibert, I. H. Guerin, I. Kuti, S. Lukyanov, A. Lepailleur, V. Maslov, P. Morfouace, J. Mrazek, F. Negoita, M. Niikura, L. Perrot, Z. Podolyák, C. Petrone, Y. Penionzhkevich, T. Roger, F. Rotaru, D. Sohler, I. Stefan, J. C. Thomas, Z. Vajta, and E. Wilson, *Phys. Rev. C* **93**, 044333 (2016).
- [15] R. F. Garcia Ruiz, M. L. Bissell, K. Blaum, A. Ekström, N. Frömmgen, G. Hagen, M. Hammen, K. Hebel, J. D. Holt, G. R. Jansen, M. Kowalska, K. Kreim, W. Nazarewicz, R. Neugart, G. Neyens, W. Nörtershäuser, T. Papenbrock, J. Papuga, A. Schwenk, J. Simonis, K. A. Wendt, and D. T. Yordanov, *Nature Physics* **12**, 594 (2016).
- [16] M. Enciu, H. N. Liu, A. Obertelli, P. Doornenbal, F. Nowacki, K. Ogata, A. Poves, K. Yoshida, N. L. Achouri, H. Baba, F. Browne, D. Calvet, F. Château, S. Chen, N. Chiga, A. Corsi, M. L. Cortés, A. Delbart, J.-M. Gheller, A. Giganon, A. Gillibert, C. Hilaire, T. Isobe, T. Kobayashi, Y. Kubota, V. Lapoux, T. Motobayashi, I. Murray, H. Otsu, V. Panin, N. Paul, W. Rodriguez, H. Sakurai, M. Sasano, D. Steppenbeck, L. Stuhl, Y. L. Sun, Y. Togano, T. Uesaka, K. Wimmer, K. Yoneda, O. Aktas, T. Aumann, L. X. Chung, F. Flavigny, S. Franchoo, I. Gasparic, R.-B. Gerst, J. Gibelin, K. I. Hahn, D. Kim, Y. Kondo, P. Koseoglou, J. Lee, C. Lehr, P. J. Li, B. D. Linh, T. Lokotko, M. MacCormick, K. Moschner, T. Nakamura, S. Y. Park, D. Rossi, E. Sahin, P.-A. Söderström, D. Sohler, S. Takeuchi, H. Toernqvist, V. Vaquero, V. Wagner, S. Wang, V. Werner, X. Xu, H. Yamada, D. Yan, Z. Yang, M. Yasuda, and L. Zanetti, *Phys. Rev. Lett.* **129**, 262501 (2022).
- [17] J. Bonnard, S. M. Lenzi, and A. P. Zuker, *Phys. Rev. Lett.* **116**, 212501 (2016).
- [18] M. Williams-Norton and R. Abegg, *Nucl. Phys. A* **291**, 429 (1977).
- [19] J. Hanspal, N. Clarke, R. Griffiths, O. Karban, and S. Roman, *Nucl. Phys. A* **436**, 236 (1985).
- [20] D. Dinca, R. V. F. Janssens, A. Gade, D. Bazin, R. Broda, B. A. Brown, C. M. Campbell, M. P. Carpenter, P. Chowdhury, J. M. Cook, A. N. Deacon, B. Fornal, S. J. Freeman, T. Glasmacher, M. Honma, F. G. Kondev, J.-L. Lecouey, S. N. Liddick, P. F. Mantica, W. F. Mueller, H. Olliver, T. Otsuka, J. R. Terry, B. A. Tomlin, and K. Yoneda, *Phys. Rev. C* **71**, 041302(R) (2005).

- [21] A. Goldkuhle, C. Fransen, A. Blazhev, M. Beckers, B. Birkenbach, T. Braunroth, E. Clément, A. Dewald, J. Dudouet, J. Eberth, H. Hess, B. Jacquot, J. Jolie, Y.-H. Kim, A. Lemasson, S. M. Lenzi, H. J. Li, J. Litzinger, C. Michelagnoli, C. Müller-Gatermann, B. S. Nara Singh, R. M. Pérez-Vidal, D. Ralet, P. Reiter, A. Vogt, N. Warr, K. O. Zell, A. Ataç, D. Barrientos, C. Barthe-Dejean, G. Benzoni, A. J. Boston, H. C. Boston, P. Bourgault, I. Burrows, J. Cacitti, B. Cederwall, M. Ciemala, D. M. Cullen, G. De France, C. Domingo-Pardo, J.-L. Foucher, G. Fremont, A. Gadea, P. Gangnant, V. González, J. Goupil, C. Henrich, C. Houarner, M. Jean, D. S. Judson, A. Korichi, W. Korten, M. Labiche, A. Lefevre, L. Legéard, F. Legruel, S. Leoni, J. Ljungvall, A. Maj, C. Maugeais, L. Ménager, N. Ménard, R. Menegazzo, D. Mengoni, B. Million, H. Munoz, D. R. Napoli, A. Navin, J. Nyberg, M. Ozille, Z. Podolyak, A. Pullia, B. Raine, F. Recchia, J. Ropert, F. Saillant, M. D. Salsac, E. Sanchis, C. Schmitt, J. Simpson, C. Spitaels, O. Stezowski, C. Theisen, M. Toulemonde, M. Tripon, J.-J. Valiente Dobón, G. Voltolini, and M. Zienińska (AGATA Collaboration), *Phys. Rev. C* **100**, 054317 (2019).
- [22] J. Prisciandaro, P. Mantica, B. Brown, D. Anthony, M. Cooper, A. Garcia, D. Groh, A. Komives, W. Kumarasiri, P. Lofy, A. Oros-Peusquens, S. Tabor, and M. Wiedeking, *Physics Letters B* **510**, 17 (2001).
- [23] Z. Meisel, S. George, S. Ahn, J. Browne, D. Bazin, B. A. Brown, J. F. Carpino, H. Chung, R. H. Cyburt, A. Estradé, M. Famiano, A. Gade, C. Langer, M. Matoš, W. Mittig, F. Montes, D. J. Morrissey, J. Pereira, H. Schatz, J. Schatz, M. Scott, D. Shapira, K. Smith, J. Stevens, W. Tan, O. Tarasov, S. Towers, K. Wimmer, J. R. Winkelbauer, J. Yurkon, and R. G. T. Zegers, *Phys. Rev. Lett.* **114**, 022501 (2015).
- [24] M. Mougeot, D. Atanasov, C. Barbieri, K. Blaum, M. Breitenfeld, A. de Roubin, T. Duguet, S. George, F. Herfurth, A. Herlert, J. D. Holt, J. Kartheim, D. Lunney, V. Manea, P. Navrátil, D. Neidherr, M. Rosenbusch, L. Schweikhard, A. Schwenk, V. Somà, A. Welker, F. Wienholtz, R. N. Wolf, and K. Zuber, *Phys. Rev. C* **102**, 014301 (2020).
- [25] A. Gade, D. Bazin, C. M. Campbell, J. A. Church, D. C. Dinca, J. Enders, T. Glasmacher, Z. Hu, K. W. Kemper, W. F. Mueller, H. Olliver, B. C. Perry, L. A. Riley, B. T. Roeder, B. M. Sherrill, and J. R. Terry, *Phys. Rev. C* **68**, 014302 (2003).
- [26] R. Winkler, A. Gade, T. Baugher, D. Bazin, B. A. Brown, T. Glasmacher, G. F. Grinyer, R. Meharchand, S. McDaniel, A. Ratkiewicz, and D. Weisshaar, *Phys. Rev. Lett.* **108**, 182501 (2012).
- [27] H. N. Liu, A. Obertelli, P. Doornenbal, C. A. Bertulani, G. Hagen, J. D. Holt, G. R. Jansen, T. D. Morris, A. Schwenk, R. Stroberg, N. Achouri, H. Baba, F. Browne, D. Calvet, F. Château, S. Chen, N. Chiga, A. Corsi, M. L. Cortés, A. Delbart, J.-M. Gheller, A. Giganon, A. Gillibert, C. Hilaire, T. Isobe, T. Kobayashi, Y. Kubota, V. Lapoux, T. Motobayashi, I. Murray, H. Otsu, V. Panin, N. Paul, W. Rodriguez, H. Sakurai, M. Sasano, D. Steppenbeck, L. Stuhl, Y. L. Sun, Y. Togano, T. Uesaka, K. Wimmer, K. Yoneda, O. Aktas, T. Aumann, L. X. Chung, F. Flavigny, S. Franchoo, I. Gašparić, R.-B. Gerst, J. Gibelin, K. I. Hahn, D. Kim, T. Koiwai, Y. Kondo, P. Koseoglou, J. Lee, C. Lehr, B. D. Linh, T. Lokotko, M. MacCormick, K. Moschner, T. Nakamura, S. Y. Park, D. Rossi, E. Sahin, D. Sohler, H. Törnqvist, V. Vaquero, V. Wagner, S. Wang, V. Werner, X. Xu, H. Yamada, D. Yan, Z. Yang, M. Yasuda, and L. Zanetti, *Phys. Rev. Lett.* **122**, 072502 (2019).
- [28] D. Steppenbeck, S. Takeuchi, N. Aoi, P. Doornenbal, M. Matsushita, H. Wang, Y. Utsuno, H. Baba, S. Go, J. Lee, K. Matsui, S. Michimasa, T. Motobayashi, D. Nishimura, T. Otsuka, H. Sakurai, Y. Shiga, N. Shimizu, P.-A. Söderström, T. Sumikama, R. Taniuchi, J. J. Valiente-Dobón, and K. Yoneda, *Phys. Rev. Lett.* **114**, 252501 (2015).
- [29] M. L. Cortés, P. Doornenbal, M. Dupuis, S. M. Lenzi, F. Nowacki, A. Obertelli, S. Péru, N. Pietralla, V. Werner, K. Wimmer, G. Authélet, H. Baba, D. Calvet, F. Château, A. Corsi, A. Delbart, J.-M. Gheller, A. Gillibert, T. Isobe, V. Lapoux, C. Louchart, M. Matsushita, S. Momiyama, T. Motobayashi, M. Niikura, H. Otsu, C. Péron, A. Peyaud, E. C. Pollacco, J.-Y. Roussé, H. Sakurai, C. Santamaria, M. Sasano, Y. Shiga, S. Takeuchi, R. Taniuchi, T. Uesaka, H. Wang, K. Yoneda, F. Browne, L. X. Chung, Z. Dombrádi, S. Franchoo, F. Giacoppo, A. Gottardo, K. Hadynska-Klek, Z. Korkulu, S. Koyama, Y. Kubota, J. Lee, M. Lettmann, R. Lozeva, K. Matsui, T. Miyazaki, S. Nishimura, L. Olivier, S. Ota, Z. Patel, E. Sahin, C. M. Shand, P.-A. Söderström, I. Stefan, D. Steppenbeck, T. Sumikama, D. Suzuki, Z. Vajta, J. Wu, and Z. Xu, *Phys. Rev. C* **97**, 044315 (2018).
- [30] L. Gaudefroy, O. Sorlin, D. Beaumel, Y. Blumenfeld, Z. Dombrádi, S. Fortier, S. Franchoo, M. Gelin, J. Gibelin, S. Grévy, F. Hammache, F. Ibrahim, K. Kemper, K. L. Kratz, S. M. Lukyanov, C. Monrozeau, L. Nalpas, F. Nowacki, A. N. Ostrowski, Y. E. Penionzhkevich, E. Pollacco, P. Roussel-Chomaz, E. Rich, J. A. Scarpaci, M. G. St. Laurent, T. Rauscher, D. Sohler, M. Stanoiu, E. Tryggstad, and D. Verney, *Eur. Phys. J. A* **27**, 309 (2006).
- [31] S. Péru, M. Girod, and J. F. Berger, *Eur. Phys. J. A* **9**, 35 (2000).
- [32] R. Rodríguez-Guzmán, J. L. Egido, and L. M. Robledo, *Phys. Rev. C* **65**, 024304 (2002).
- [33] S. Hilaire and M. Girod, *Eur. Phys. J. A* **33**, 237 (2007).
- [34] <http://www-phynu.cea.fr>.
- [35] J. P. Delaroche, M. Girod, J. Libert, H. Goutte, S. Hilaire, S. Péru, N. Pillet, and G. F. Bertsch, *Phys. Rev. C* **81**, 014303 (2010).
- [36] B. D. Linh, A. Corsi, A. Gillibert, A. Obertelli, P. Doornenbal, C. Barbieri, S. Chen, L. X. Chung, T. Duguet, M. Gómez-Ramos, J. D. Holt, A. Moro, P. Navrátil, K. Ogata, N. T. T. Phuc, N. Shimizu, V. Somà, Y. Utsuno, N. L. Achouri, H. Baba, F. Browne, D. Calvet, F. Château, N. Chiga, M. L. Cortés, A. Delbart, J.-M. Gheller, A. Giganon, C. Hilaire, T. Isobe, T. Kobayashi, Y. Kubota, V. Lapoux, H. N. Liu, T. Motobayashi, I. Murray, H. Otsu, V. Panin, N. Paul, W. Rodriguez, H. Sakurai, M. Sasano, D. Steppenbeck, L. Stuhl, Y. L. Sun, Y. Togano, T. Uesaka, K. Wimmer, K. Yoneda, O. Aktas, T. Aumann, F. Flavigny, S. Franchoo, I. Gašparić, R.-B. Gerst, J. Gibelin, K. I. Hahn, N. T. Khai, D. Kim, T. Koiwai, Y. Kondo, P. Koseoglou, J. Lee, C. Lehr, T. Lokotko, M. MacCormick, K. Moschner, T. Nakamura, S. Y. Park, D. Rossi, E. Sahin, D. Sohler,

- P.-A. Söderström, S. Takeuchi, N. D. Ton, H. Törnqvist, V. Vaquero, V. Wagner, H. Wang, V. Werner, X. Xu, Y. Yamada, D. Yan, Z. Yang, M. Yasuda, and L. Zanetti, *Phys. Rev. C* **104**, 044331 (2021).
- [37] T. Kubo, D. Kameda, H. Suzuki, N. Fukuda, H. Takeda, Y. Yanagisawa, M. Ohtake, K. Kusaka, K. Yoshida, N. Inabe, T. Ohnishi, A. Yoshida, K. Tanaka, and Y. Mizoi, *Prog. Theor. Exp. Phys* **2012** (2012).
- [38] N. Fukuda, T. Kubo, T. Ohnishi, N. Inabe, H. Takeda, D. Kameda, and H. Suzuki, *Nucl. Instrum. Methods Phys. Res. B* **317**, 323 (2013).
- [39] Obertelli, A., Delbart, A., Anvar, S., Audirac, L., Authélet, G., Baba, H., Bruyneel, B., Calvet, D., Château, F., Corsi, A., Doornenbal, P., Gheller, J.-M., Giganon, A., Lahonde-Hamdoun, C., Leboeuf, D., Loiseau, D., Mohamed, A., Mols, J.-Ph., Otsu, H., Péron, C., Peyaud, A., Pollacco, E. C., Prono, G., Rousse, J.-Y., Santamaria, C., and Uesaka, T., *Eur. Phys. J. A* **50**, 8 (2014).
- [40] T. Kobayashi, N. Chiga, T. Isobe, Y. Kondo, T. Kubo, K. Kusaka, T. Motobayashi, T. Nakamura, J. Ohnishi, H. Okuno, H. Otsu, T. Sako, H. Sato, Y. Shimizu, K. Sekiguchi, K. Takahashi, R. Tanaka, and K. Yoneda, *Nucl. Instrum. Methods Phys. Res. B* **317**, 294 (2013).
- [41] S. Takeuchi, T. Motobayashi, Y. Togano, M. Matsushita, N. Aoi, K. Demichi, H. Hasegawa, and H. Murakami, *Nucl. Instrum. Methods Phys. Res. A* **763**, 596 (2014).
- [42] M. Wang, W. Huang, F. Kondev, G. Audi, and S. Naimi, *Chin. Phys. C* **45**, 030003 (2021).
- [43] K. Boretzky, I. Gašparić, M. Heil, J. Mayer, A. Heinz, C. Caesar, D. Kresan, H. Simon, H. Törnqvist, D. Körper, G. Alkhazov, L. Atar, T. Aumann, D. Bemmerer, S. Bondarev, L. Bott, S. Chakraborty, M. Cherciu, L. Chulkov, M. Ciobanu, U. Datta, E. De Filippo, C. Douma, J. Dreyer, Z. Elekes, J. Enders, D. Galaviz, E. Geraci, B. Gnoffo, K. Göbel, V. Golovtsov, D. Gonzalez Diaz, N. Gruzinsky, T. Heftrich, H. Heggen, J. Hehner, T. Hensel, E. Hoemann, M. Holl, A. Horvat, A. Horváth, G. Ickert, D. Jelavić Malenica, H. Johansson, B. Jonson, J. Kahlbow, N. Kalantar-Nayestanaki, A. Kelić-Heil, M. Kempe, K. Koch, N. Kozlenko, A. Krivshich, N. Kurz, V. Kuznetsov, C. Langer, Y. Leifels, I. Lihtar, B. Löher, J. Machado, N. Martorana, K. Miki, T. Nilsson, E. Orischin, E. Pagano, S. Pirrone, G. Politi, P.-M. Potlog, A. Rahaman, R. Reifarh, C. Rigollet, M. Röder, D. Rossi, P. Russotto, D. Savran, H. Scheit, F. Schindler, D. Stach, E. Stan, J. Stomvall Gill, P. Teubig, M. Trimarchi, L. Uvarov, M. Volkmandt, S. Volkov, A. Wagner, V. Wagner, S. Wranne, D. Yakorev, L. Zanetti, A. Zilges, and K. Zuber, *Nucl. Instrum. Methods Phys. Res. A* **1014**, 165701 (2021).
- [44] T. Nakamura and Y. Kondo, *Nucl. Instrum. Methods Phys. Res. B* **376**, 156 (2016).
- [45] S. Chen, J. Lee, P. Doornenbal, A. Obertelli, C. Barbieri, Y. Chazono, P. Navrátil, K. Ogata, T. Otsuka, F. Raimondi, V. Somà, Y. Utsuno, K. Yoshida, H. Baba, F. Browne, D. Calvet, F. Château, N. Chiga, A. Corsi, M. L. Cortés, A. Delbart, J.-M. Gheller, A. Giganon, A. Gillibert, C. Hilaire, T. Isobe, J. Kahlbow, T. Kobayashi, Y. Kubota, V. Lapoux, H. N. Liu, T. Motobayashi, I. Murray, H. Otsu, V. Panin, N. Paul, W. Rodriguez, H. Sakurai, M. Sasano, D. Steppenbeck, L. Stuhl, Y. L. Sun, Y. Togano, T. Uesaka, K. Wimmer, K. Yoneda, N. Achouri, O. Aktas, T. Aumann, L. X. Chung, F. Flavigny, S. Franchoo, I. Gašparić, R.-B. Gerst, J. Gibelin, K. I. Hahn, D. Kim, T. Koiwai, Y. Kondo, P. Koseoglou, C. Lehr, B. D. Linh, T. Lokotko, M. MacCormick, K. Moschner, T. Nakamura, S. Y. Park, D. Rossi, E. Sahin, D. Sohler, P.-A. Söderström, S. Takeuchi, H. Törnqvist, V. Vaquero, V. Wagner, S. Wang, V. Werner, X. Xu, H. Yamada, D. Yan, Z. Yang, M. Yasuda, and L. Zanetti, *Phys. Rev. Lett.* **123**, 142501 (2019).
- [46] Y. Sun, A. Obertelli, P. Doornenbal, C. Barbieri, Y. Chazono, T. Duguet, H. Liu, P. Navrátil, F. Nowacki, K. Ogata, T. Otsuka, F. Raimondi, V. Somà, Y. Utsuno, K. Yoshida, N. Achouri, H. Baba, F. Browne, D. Calvet, F. Château, S. Chen, N. Chiga, A. Corsi, M. Cortés, A. Delbart, J.-M. Gheller, A. Giganon, A. Gillibert, C. Hilaire, T. Isobe, T. Kobayashi, Y. Kubota, V. Lapoux, T. Motobayashi, I. Murray, H. Otsu, V. Panin, N. Paul, W. Rodriguez, H. Sakurai, M. Sasano, D. Steppenbeck, L. Stuhl, Y. Togano, T. Uesaka, K. Wimmer, K. Yoneda, O. Aktas, T. Aumann, L. Chung, F. Flavigny, S. Franchoo, I. Gašparić, R.-B. Gerst, J. Gibelin, K. Hahn, D. Kim, T. Koiwai, Y. Kondo, P. Koseoglou, J. Lee, C. Lehr, B. Linh, T. Lokotko, M. MacCormick, K. Moschner, T. Nakamura, S. Park, D. Rossi, E. Sahin, D. Sohler, P.-A. Söderström, S. Takeuchi, H. Törnqvist, V. Vaquero, V. Wagner, S. Wang, V. Werner, X. Xu, H. Yamada, D. Yan, Z. Yang, M. Yasuda, and L. Zanetti, *Phys. Lett. B* **802**, 135215 (2020).
- [47] A. M. Moro, *Phys. Rev. C* **92**, 044605 (2015).
- [48] T. Wakasa, K. Ogata, and T. Noro, *Prog. in Part. and Nucl. Phys.* **96**, 32 (2017).
- [49] T. Aumann, C. A. Bertulani, and J. Ryckebusch, *Phys. Rev. C* **88**, 064610 (2013).
- [50] K. Ogata, K. Yoshida, and K. Minomo, *Phys. Rev. C* **92**, 034616 (2015).
- [51] R. E. Kass and A. E. Raftery, *J. Am. Stat. Assoc.* **90**, 773 (1995).
- [52] I. Murray, F. Browne, S. Chen, M. L. Cortés, P. Doornenbal, H. Sakurai, J. Lee, M. MacCormick, W. Rodriguez, V. Vaquero, D. Steppenbeck, and K. Wimmer, *RIKEN Accel. Prog. Rep.* **51**, 148 (2018).
- [53] T. Aumann, C. Barbieri, D. Bazin, C. Bertulani, A. Bonaccorso, W. Dickhoff, A. Gade, M. Gómez-Ramos, B. Kay, A. Moro, T. Nakamura, A. Obertelli, K. Ogata, S. Paschalis, and T. Uesaka, *Prog. in Part. and Nucl. Phys.* **118**, 103847 (2021).
- [54] M. Gómez-Ramos and A. Moro, *Phys. Lett. B* **785**, 511 (2018).
- [55] S. Goriely, S. Hilaire, M. Girod, and S. Péru, *Phys. Rev. Lett.* **102**, 242501 (2009).
- [56] J. Dechargé and D. Gogny, *Phys. Rev. C* **21**, 1568 (1980).
- [57] Y. Utsuno, T. Otsuka, B. A. Brown, M. Honma, T. Mizusaki, and N. Shimizu, *Phys. Rev. C* **86**, 051301(R) (2012).
- [58] S. Péru and M. Martini, *Eur. Phys. J. A* **50**, 88 (2014).
- [59] S. Goriely, S. Péru, G. Colò, X. Roca-Maza, I. Gheorghe, D. Filipescu, and H. Utsunomiya, *Phys. Rev. C* **102**, 064309 (2020).
- [60] S. R. Stroberg, H. Hergert, S. K. Bogner, and J. D. Holt, *Annu. Rev. Nucl. Part. Sci.* **69**, 307 (2019).
- [61] V. Somà, T. Duguet, and C. Barbieri, *Phys. Rev. C* **84**, 064317 (2011).
- [62] V. Somà, *Front. Phys.* **8**, 340 (2020).

- 1334 [63] S. R. Stroberg, A. Calci, H. Hergert, J. D. Holt, S. K. 1345
1335 Bogner, R. Roth, and A. Schwenk, *Phys. Rev. Lett.* **118**, 1346
1336 032502 (2017). 1347
- 1337 [64] T. Miyagi, S. R. Stroberg, P. Navrátil, K. Hebeler, and 1348
1338 J. D. Holt, *Phys. Rev. C* **105**, 014302 (2022). 1349
- 1339 [65] S. R. Stroberg, Private communication (2021) (). 1350
- 1340 [66] K. Hebeler, S. K. Bogner, R. J. Furnstahl, A. Nogga, and 1351
1341 A. Schwenk, *Phys. Rev. C* **83**, 031301(R) (2011). 1352
- 1342 [67] W. G. Jiang, A. Ekström, C. Forssén, G. Hagen, G. R. 1353
1343 Jansen, and T. Papenbrock, *Phys. Rev. C* **102**, 054301 1354
1344 (2020).
- [68] V. Somà, P. Navrátil, F. Raimondi, C. Barbieri, and
T. Duguet, *Phys. Rev. C* **101**, 014318 (2020).
- [69] A. Ekström, G. R. Jansen, K. A. Wendt, G. Hagen,
T. Papenbrock, B. D. Carlsson, C. Forssén, M. Hjorth-
Jensen, P. Navrátil, and W. Nazarewicz, *Phys. Rev. C*
91, 051301(R) (2015).
- [70] S. R. Stroberg, `imsrg++`, <https://github.com/ragnarstroberg/imsrg> ().
- [71] N. Shimizu, T. Mizusaki, Y. Utsuno, and Y. Tsunoda,
Comput. Phys. Commun. **244**, 372 (2019).